Universitatea Națională de Știință și Tehnologie **POLITEHNICA** București
Faculty of Materials Science and Engineering
Department of Engineering and Management of Metal Materials Processing

DOCTORAL THESIS

COMPOZITE CU MATRICE DIN ALIAJE DE ALUMINIU RANFORSATE IN-SITU CU DIBORURI DE VANADIU

ALUMINIUM ALLOY MATRIX COMPOSITES REINFORCED IN-SITU WITH VANADIUM DIBORIDES

Author
Ing. Cătălin OGICA

PhD supervisor
Prof. dr. ing. Mihai BUZATU

Bucharest, 2024

Contents

CHAPTER 1. METAL MATRIX COMPOSITES (CLASSIFICATION)

1.1. General

A metal matrix composite system is generally designated simply by the metal alloy designation of the matrix and by the material type, volume fraction and shape of the ceramic reinforcement phase [1]. For example, 6061Al/ 30v/o SiCp means a discontinuously reinforced 6061 aluminium alloy with a reinforcing phase consisting of silicon carbide particles representing 30 % by volume [1]. A continuously armed CMM can be designated by SiC_f, e.g. [1].

These names do not fully describe the composite system as they do not include information on the basic reinforcement process (metallurgical reinforcement of ingots or powders), the subsequent heat treatments applied or the spatial orientations of the fibres.

MMC differs from other composite materials in several ways. Some of these general distinctions are as follows [1]:

1. The basic metal matrix of an MMC is either a pure metal or a metal alloy, as opposed to a polymer or a ceramic.

2. MMCs exhibit higher ductility and hardness than alloys with a non-reinforced metal matrix, ceramics or CMCs.

3. The role of the reinforcement phase in MMCs is to increase mechanical strength. In general, the purpose of reinforcing MMCs is to ensure better damage tolerance.

4. MMCs have a higher service temperature than polymers and PMCs, but lower than ceramics and CMCs.

5. Weakly to moderately reinforced MMCs can be formed by processes normally associated with non-armoured metals.

Metals are extremely versatile materials, a metallic material can exhibit a wide range of properties easily controlled by appropriate selection of alloy composition and thermo-mechanical processing methods [1]. The widespread use of metal alloys in engineering reflects not only their strength and toughness, but also the relative ease and low cost of manufacturing engineering components through a wide range of manufacturing processes.

1.2. Aluminium matrix

The most commonly used matrixes are aluminium-based alloys, both deformable and casting [2].

Aluminium matrices can be plastically processed and cast by any conventional process, so that aluminium matrix composites can be obtained by casting or deformation methods (forging, rolling, extrusion) similar to those used for alloys [3].

Aluminium and aluminium-based binary alloys are generally less used as matrixes [4]. Matrices with the lowest possible content of minor alloying elements, such as Mn and Cr, are preferred, as they form intermetallic compounds during processing, which can negatively influence the mechanical characteristics [4].

The choice of matrix should take into account not only the desired properties of the composite material, but also the processing method [5]. Thus, although 7xxx series master alloys exhibit better mechanical properties (strength and stiffness) for aerospace applications than 2xxx series alloys, the latter are most often used [5]. This is due to the fact that 7xxx series alloys degrade easily at the interface with reinforcing materials (reinforcement), leading to a decrease in the mechanical characteristics of these composites [5].

2xxx, 6xxx and 7xxx series alloys are the most commonly used as dies for MMC; these alloys can be precipitation hardened [5].

1.3. Reinforcing materials

MMC reinforcing materials are discrete fibres or second-phase additions to a metal matrix that result in a net improvement in some property, usually an increase in mechanical strength and/or stiffness [6].

Most often, reinforcing materials for MMC are ceramics (oxides, carbides, nitrides, etc.), which are characterized by high mechanical strength and stiffness at both ambient and elevated temperatures [7]. Examples of the most common reinforcement phases used in metal matrix composites are SiC, Al_2O_3, TiB_2, B_4C and graphite. Metal reinforcing phases are used less frequently [8].

Reinforcing materials can be divided into two major groups: (a) particles or whiskers; and (b) fibres [9]. Fibre reinforcements can be further divided into continuous and staple fibres. Fibres increase mechanical strength in the direction of their orientation [9]. A disadvantage of continuous fibre reinforced CMMs is the low mechanical strength in the direction perpendicular to the direction of fibre orientation [10]. Discontinuously reinforced MMCs, on the other hand, exhibit several isotropic characteristics [10]. Two or more types of reinforcement phases may be present in some MMC systems to confer specific properties [10].

Long fibres (continuous)

Long-fibre reinforcement materials are generally ceramic (except wires), usually carbon, boron, oxides, carbides and nitrides [11]. They are used because they provide high mechanical strength and stiffness values at both normal and high temperatures [11].

In the direction of stress, the fibres have high mechanical strength, but in the perpendicular direction of fibre orientation the strength decreases greatly [11].

Multifilament fibres (Fig. 1.4) are made of C, SiC and Al2O3, while monofilament fibres are made of boron [11].

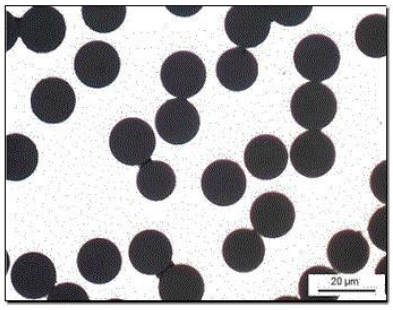

Figure 1.4. Micrograph of an Al matrix composite reinforced with 40% Altex fibres (85% Al_2O_3) [11]

Small diameter continuous fibres (5-30 μm) are often described as multifilaments. These multifilaments are flexible enough to be braided into cables [11]. These include SiC, C and various oxide systems [11].

Short fibres (discontinuous) and whiskers

Short (discontinuous) fibre reinforcement materials can be oriented (aligned) or randomly distributed in metal matrices (Fig.1.5) [12].

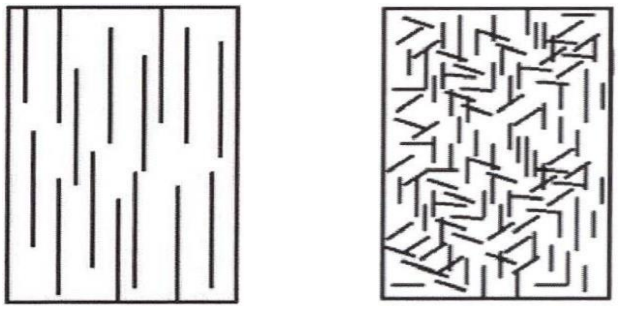

Figure 1.5. Orientation of short staple fibres in metal matrices: (a) aligned fibres; (b) randomly oriented fibres [12].

Aligned short fibres are longer than the critical length (l_c) [12]:

$$\boldsymbol{l_c = d \cdot S_f / S_m} \qquad (1.1)\ [43]$$

where: d is the fibre diameter, S_f and S_m are the tensile strengths of the fibres and matrix respectively [12].

Under these conditions the mechanical strength of MMC reinforced with aligned short fibres is high. The short fibres (diameter greater than 1 μm) have an aspect ratio above 5, but this can reach even above 100 [13].

The most commonly used short fibres are those made from alumino-silicates; the best known trade name is Saffil (Fig. 1.6.) [12]. These fibres have a polycrystalline microstructure. The mechanical properties of MMC reinforced with these fibres are superior to composites reinforced with particles [12].

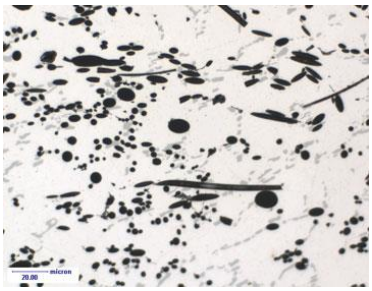

Figure 1.6. Composite AlSi10/15%vol. SAFFIL fibres, cast state [12].

Superior mechanical properties of MMC are achieved if the fine-grained structure of the short fibres is replaced by a single crystal [12]. Single crystals of short fibres are known as whiskers [12]. Reinforcing materials are elongated single crystals with aspect ratios greater than 10 (usually several hundred) and diameters less than 1 μm [12].

Ceramic particles

Ceramic particles are the most widely used reinforcement materials mainly due to their low cost [14].

The first MMC composites were made from matrices of aluminium alloys and graphite particles, incorporated at <10%vol [15]. MMCs with a high volume percentage of various ceramic reinforcement particles (oxides, nitrides, carbides, etc.) are currently produced. [15].

CHAPTER 2. Production/processing techniques used in the manufacture/production of metal matrix composites

The choice of primary manufacturing process for the development of any metal matrix composite is dictated by several factors, the most important of which are [16]:

1. Maintaining the strength of the reinforcement phase
2. Minimising damage to the reinforcement phase
3. Promote wetting and bonding between matrix and reinforcement
4. Flexibility to allow proper support, spacing and orientation of reinforcement within the matrix [17].

2.1. Fabrication procedures

Infiltration of liquid metal

Preforms are infiltrated with liquid metal using gravity, vacuum or high pressure (Fig 2.1).

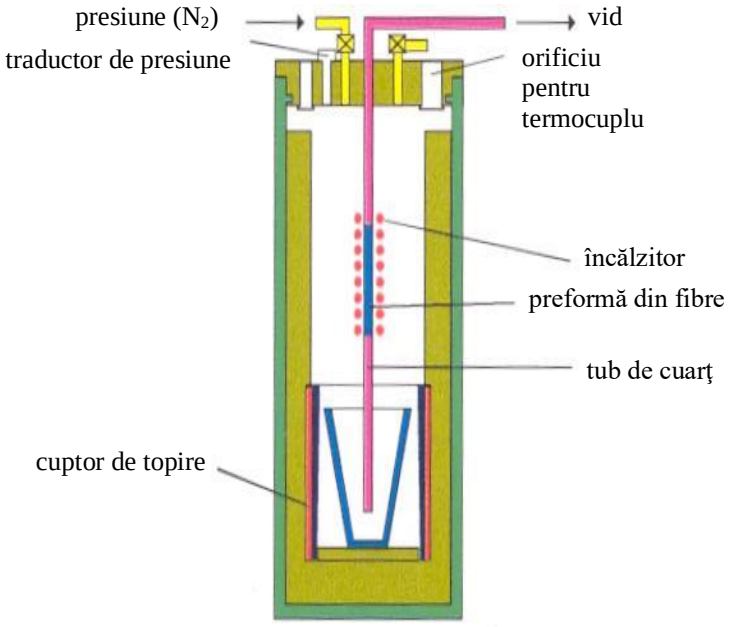

Figure 2.1. Infiltration technique of continuous fibre preform.

Liquid state processing

The simplest technique for dispersing ceramic particles in the liquid matrix is the VORTEX method, which consists of intense agitation of the melt with the solid particles (Fig. 2.6).

.

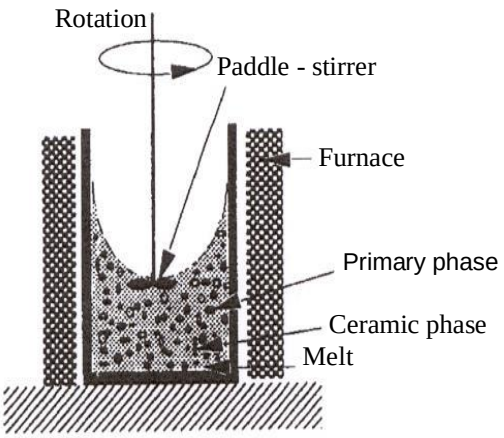

Figure 2.6. Mechanical agitation of ceramic particles in solid + liquid alloy mixture

The incorporation of ceramic particles into the liquid matrix by the stirring technique takes place in several stages. The particles added in the vortex to the surface of the melt are gradually moistened and have an incubation period until they are incorporated into the melt. Partially wetted particles gradually penetrate through the gas layer between particles or clusters. Fully wetted ceramic particles are uniformly dispersed in the liquid matrix.

Casting of composite materials (MMC) can be done gravitationally, in moulds from forming mixtures or in metal shells and centrifugal casting.

Casting Processes (Liquid Forging)

Squeeze casting is a technique used in the manufacture of liquid-phase composites using preforms made of reinforcing material. It consists of infiltration under unidirectional pressure (pressure 70 - 150 MPa). The final parts contain no porosities and have a microstructure with small equiaxial grains. The infiltration rate depends on the applied pressure, capillarity, distance between dispersed particles, liquid metal viscosity, shape permeability, mould, preform and melt temperatures.

The infiltration technology flow is shown in Fig. 2.8.

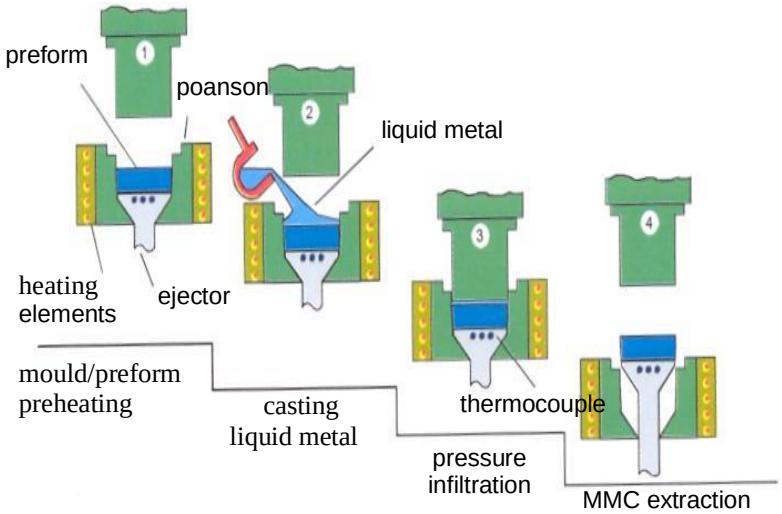

Figure 2.8. Technological flow of the Squeeze Casting infiltration process

In-situ production processes

In-situ processes for obtaining MMC do not require initial reinforcing materials [18]. In these processes the reinforcing material is formed from in-situ reactions in the metal matrix in a single phase [18]. Another advantage is that the interfaces between the reinforcing material and the matrix are very clean, allowing better wetting and bonding between the matrix and the reinforcing material (no gas adsorption, no oxidation, no reactions at the interface) [18]. Costs and hazards are also reduced, as handling operations of fine particles of reinforcing material are eliminated [18].

The main processes are: injection of gases or salts into the metal matrix, reactive infiltration of the liquid matrix into a porous preform, unidirectional solidification of eutectic alloys [18].

2.2. Areas of use of composite materials

Due to the combination of excellent properties such as high mechanical strength and stiffness, high thermal stability, low coefficient of thermal expansion and high wear resistance as well as continuous cost reduction, MMC composites are becoming more and more popular in various fields such as: transportation industry, aerospace industry, electronics industry and production of sports materials (e.g. bicycles) [19] [20] [21] [22].

Applications in the transport industry

A large number of components for cars and other vehicles such as pistons, cylinder liners, connecting rods, brake discs and rotors, calipers, universal joints, are made of metal matrix composite materials, mainly aluminium-based. The main composite materials belong to the Al-SiC, Al-Al_2O_3, Mg-SiC, Mg-Al_2O_3 systems, the reinforcement materials being ceramic particles or short fibres [23] [24].

Fig. 2.12 shows a diesel engine piston made by squeeze-casting from Al/Al_2O_3(short fibre) composite, and Fig. 2.13 shows brake rotors for high-speed trains in underground (subway) and rail transport as well as brake discs for cars. Brake rotors are made of AlSi7Mg/20% vol. SiC; their mass is only 76 kg compared to the mass of conventional rotors weighing 120 kg [25].

Figure 2.12. Short fibre reinforced aluminium matrix composite piston for diesel engines [12].

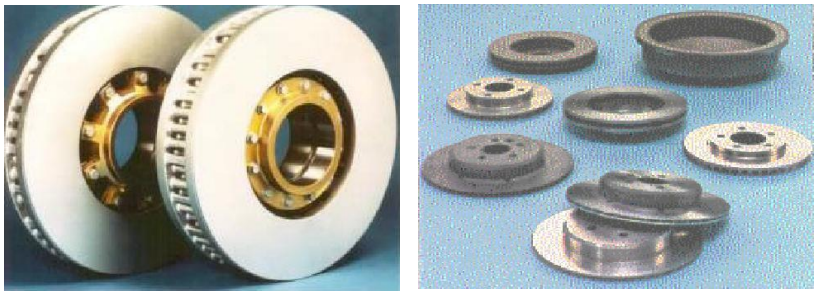

(a) (b)

Figure 2.13. Brake rotors for high-speed trains (a) and braking systems for cars (b) [12].

Applications in the electronics industry

Advances in microelectronics have led to the development of miniaturised devices in which aluminium matrix composites reinforced with ceramic particles play an increasingly important role [26]. This is due to low coefficient of thermal expansion, high thermal conductivity, low density and low cost [26].

Fig. 2.14 shows a multichip module fabricated by pressure infiltration from Al/65-75%vol composite. SiC [27].

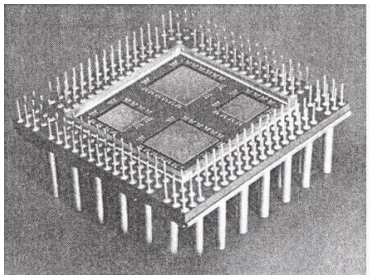

Figure 2.14. Electronic multichip module made of Al/SiCp composite [27]

2.3. Recycling

Important examples of MMC products currently marketed are diesel engine pistons [28], engine pistons [29] and automotive cylinder blocks [30] [31]. The volume of the composite part of these products is very small [32]. For example, in the case of diesel engine pistons, only the part surrounding the piston ring is made of composite. The reinforcing phase of this part consists of short alumina/silica fibres (diameter about 3 mm) and the volume fraction of the fibres is 7-8 %. The composite part of automotive cylinder blocks is the inner surface of the cylinder; they are 3 mm thick and contain about 20 % vol. fibres. The fibres used for the cylinder block are short alumina fibres (diameter about 3 mm) and carbon fibres (diameter about 7 mm) [33].

When the composite scrap is melted, the composite piece sinks to the bottom of the crucible, retaining its original shape, because the reinforcing fibers usually have a higher specific gravity than the matrix metal and each fiber does not move separately in the melt [34].

However, technologies to separate the reinforcement particles from the matrix metal will be important for matrix metal recovery [31].

CHAPTER 3. Development of AA6063/VB_2 composites by in situ reactions

In the field of academic research, multiple studies have been documented on the production of aluminium alloy matrix composites of the AA7075, A356, AA2024, AA5052, AA2014 and AA6061 series, which have been reinforced by dispersion of zirconium diboride particles. These composites were synthesized by means of aluminothermic reactions at various temperatures (1000K, 1023K, 1123K, 1143K, 1158K, 1163K and 1173K). The process involved the use of different concentrations of KBF_4 salts for boron introduction and AlV10 for vanadium contribution.

In this study, in order to investigate the improvement of microstructures of AA6063/VB_2 metal matrix composites, VB2 reinforcement particles were obtained by in-situ synthesis method using AA6063 molten alloy with AlV10 pre-alloy and KBF_4 salt.

A number of composites have been successfully fabricated using the in situ method by the aluminothermic reaction:

$$6KBF_4 + 3V + 6Al = 3\mathbf{VB_2} + 2K_3AlF_6 + 4AlF_3 \qquad (3.1)$$

Load calculation

In order to obtain bars for tensile testing and samples for microstructure analysis, the composite melts were cast into pre-heated bar-shaped dies with ϕ = 12 mm and h = 90 mm at different VB_2 concentrations (1%, 2%, 3%, 4%, 5% and 10%).

Based on crucible capacity, it was determined that 300 g of aluminium alloy should be used for good in-situ processing of composites.

Table 3.1. Impurity-free chemical composition profile according to the standard

	Si	**Fe**	**Cu**	**Mn**	**Mg**	**Cr**	**Zn**	**Ti**
AA 6063	0.2-0.6	0.35	0.10	0.10	0.45-0.9	0.10	0.10	0.10
Nominal	0.49	0.33	0.02	0.02	0.72	0.06	0.03	0.04

The stoichiometric calculations required to obtain Al/VB_2 composites are:

Calculation for required VB_2 at 200g, 10% concentration:

$$\underset{X}{\underline{6\cdot125.908\ 6KBF_4}} + \underset{Y}{\underline{3\cdot50.941\ 3V}} + \underset{Z}{\underline{6\cdot26.98\ 6Al}} = \underset{20g}{\underline{3\cdot72.563\ 3VB_2}} + \underline{2\cdot25.824}\ 2K_3AlF_6 + \underset{W}{\underline{4\cdot83.975\ 4AlF_3}}$$

Quantities of materials used:
140 g alloy 6063 + 56 g, 140 g AlV10, 69,2 g KBF_4

Gibbs free energy formations for aluminium and vanadium borides were tested using HSC Chemistry at temperatures between 500°C and 1000°C. Figure 3.1 shows the stability curves of the different possible reactions [35].

Through thermodynamic analysis of the reactions occurring in the melt, we found that reaction (3.1) was the most likely reaction to occur during the development of the composite.

$$6KBF_4 + 3V + 6Al = 3VB_2 + 2K_3AlF_6 + 4AlF_3 \qquad (3.1)\ [35]$$

$$2KBF_4 + V + 2Al = VB_2 + 2KF + 2AlF_3 \qquad (3.2)\ [35]$$

$$3Al + 1{,}5V + Na_3AlF_6 + 3KBF_4 = 1{,}5VB_2 + K_3AlF_6 + 3AlF_3 + 3NaF \qquad (3.3)\ [35]$$

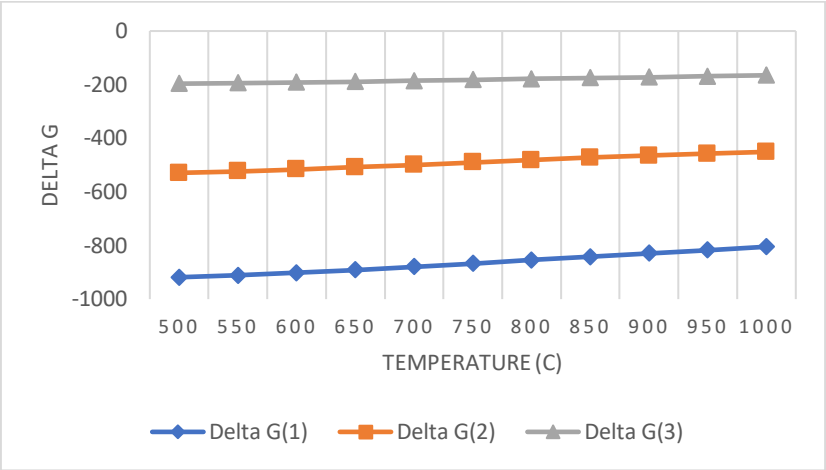

Figure 3.1. Standard free enthalpy variation in the temperature range 500 - 1000 ^{o}C of reactions 3.1 ÷ 3.3 [35]

The metallographic samples were processed using the DELTA Abrasimet cutting machine, the SIMPLIMET 1000 embedding machine and the Beta/1 Single grinding/polishing machine. The samples were then analysed using the Olympus UC30 optical microscope at different dimensions (Fig. 3.4, Fig. 3.7, Fig. 3.10, Fig. 3.13, Fig. 3.16, Fig. 3.19)..

1% VB_2

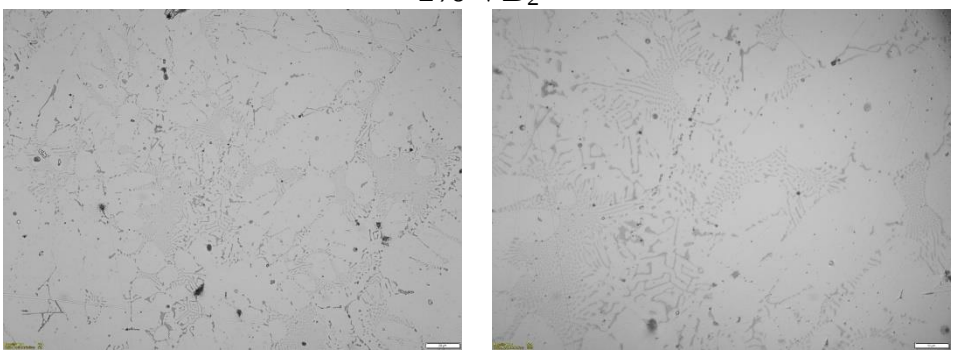

VB_2 1% x500 3 VB_2 1% x1000 1

Figure 3.4 Optical microscopy analysis of composites with a concentration of 1% reinforcement particles [35]

Phase analysis:

Phase analysis was performed using **DIFFRAC.EVA** release 2019 software and the **ICDD PDF4+ 2020 database.**

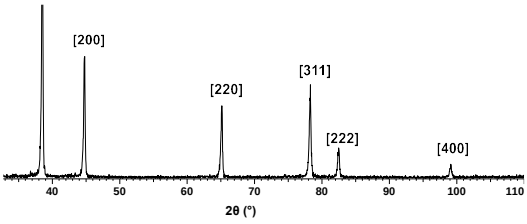

Figure 3.6. Graphical presentation of qualitative XRD phase analysis for Sample 1 [35]

Compound Name	PDF reference	Chemical formula	Crystallization system	Space Group
Ss type A1	04-017-1423	Ss Type A1- $Al_{1-x}M_x$ (prototype Cu)	Cubic (Cube with centered faces)	Fm-3m (225)

2% VB_2

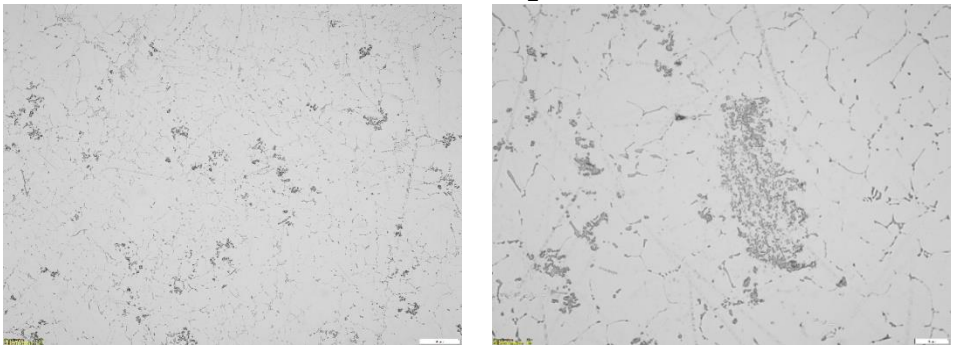

VB_2 2% x200 2 VB_2 2% x500 5

Figure 3.7 Optical microscopy analysis of composites with a concentration of 2% reinforcing particles

Phase analysis:

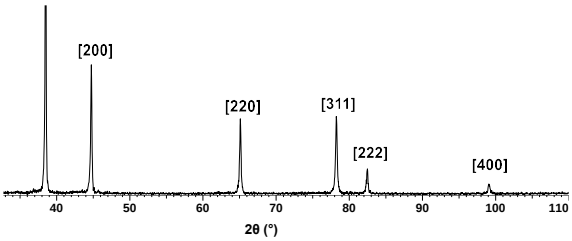

Figure 3.9 Graphical presentation of qualitative XRD phase analysis for Sample 2

Compound Name	PDF reference	Chemical formula	Crystallization system	Space Group
Ss type A1	04-017-1423	Ss Type A1- $Al_{1-x}M_x$ (prototype Cu)	Cubic (Cube with centered faces)	Fm-3m (225)

3% VB_2

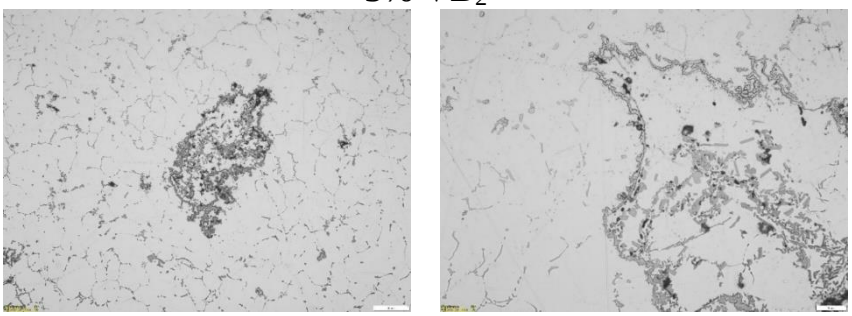

Figure 3.10 Optical microscopy analysis of composites with a concentration of 3% reinforcing particles

Phase analysis:

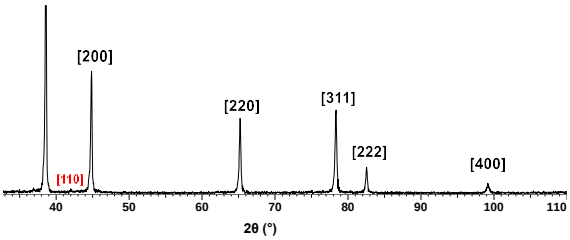

Figure 3.12 Graphical presentation of qualitative XRD phase analysis for Sample 3

Compound Name	PDF reference	Chemical formula	Crystallization system	Space Group
Ss type A1	04-017-1423	Ss Type A1- $Al_{1-x}M_x$ (prototype Cu)	Cubic (Cube with centered faces)	Fm-3m (225)
AlV_2	01-077-6859	AlV_2	Cubic (Cube with centered volume)	Im-3m (229)

4% VB_2

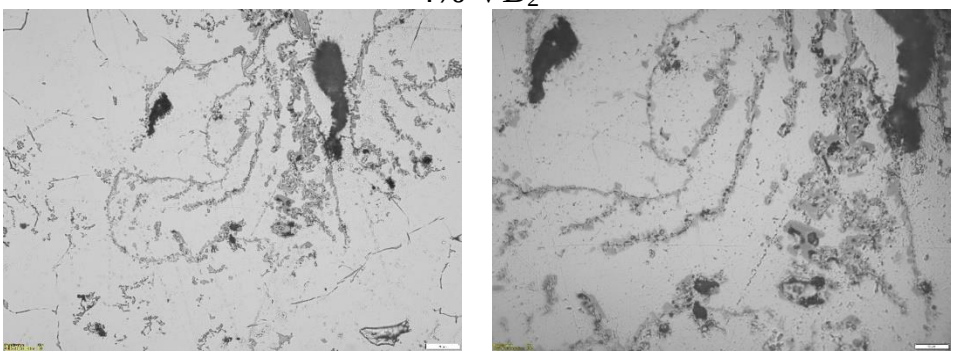

VB_2 4% x500 4 VB_2 4% x1000 1

Figure 3.13 Optical microscopy analysis of composites with a concentration of 4% reinforcing particles

Phase analysis:

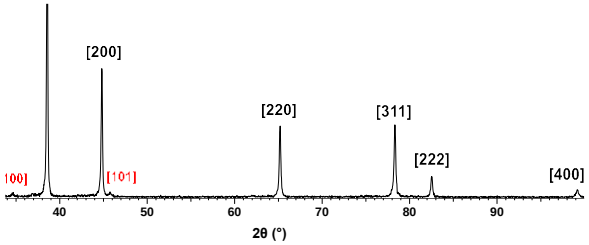

Figure 3.15 Graphical presentation of qualitative XRD phase analysis for Sample 4

Compound Name	PDF reference	Chemical formula	Crystallization system	Space Group
Ss type A1	04-017-1423	Ss Type A1- $Al_{1-x}M_x$ (prototype Cu)	Cubic (Cube with centered faces)	Fm-3m (225)
VB_2	00-038-1463	VB_2	Hexagonal	P6/mmm (191)

5% VB_2

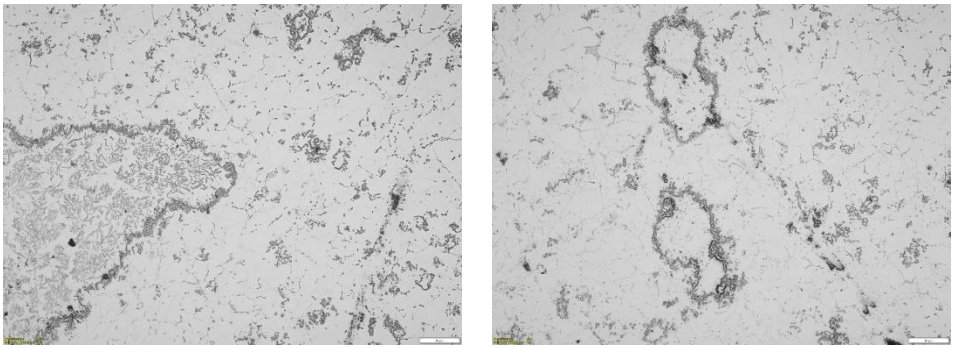

VB_2 5% x200 VB_2 5% x200

Figure 3.16 Optical microscopy analysis of composites with a concentration of 5% reinforcing particles

Phase analysis:

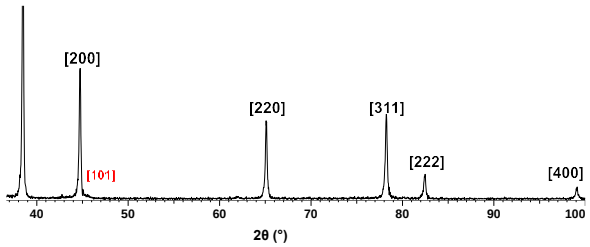

Figure 3.18 Graphical presentation of qualitative XRD phase analysis for Sample 5

Compound Name	PDF reference	Chemical formula	Crystallization system	Space Group
Ss type A1	04-017-1423	Ss Type A1- $Al_{1-x}M_x$ (prototype Cu)	Cubic (Cube with centered faces)	Fm-3m (225)
VB_2	00-038-1463	VB_2	Hexagonal	P6/mmm (191)

10% VB_2

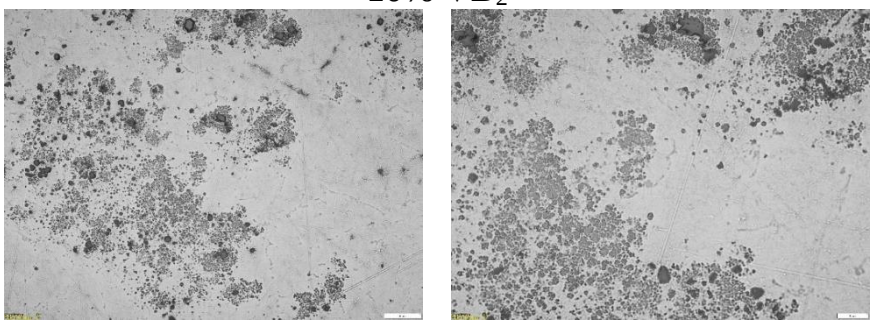

VB_2 10% x200 2 VB_2 10% x500 2

Figure 3.19 Optical microscopy analysis of composites with a concentration of 10% reinforcement particles

Phase analysis:

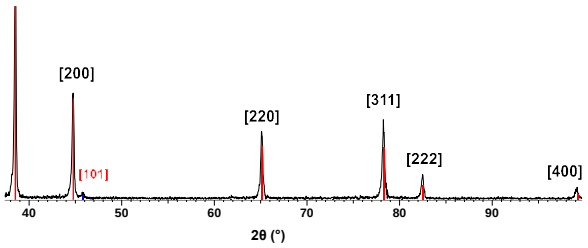

Figure 3.21 Graphical presentation of qualitative XRD phase analysis for Sample 6

Compound Name	PDF reference	Chemical formula	Crystallization system	Space Group
Ss type A1	04-017-1423	Ss Type A1- $Al_{1-x}M_x$ (prototype Cu)	Cubic (Cube with centered faces)	Fm-3m (225)
VB_2	00-038-1463	VB_2	Hexagonal	P6/mmm (191)

In the study, VB2 and Al compounds were found in all composite samples. The D8 ADVANCE diffractometer is a unique platform in the D8 family of diffractometers, ideally suited for a variety of X-ray diffraction and scattering applications, including X-ray diffraction (XRD), pair distribution function analysis (PDF analysis), wide and small angle X-ray scattering (SAXS, WAXS) (Figure 3.22).

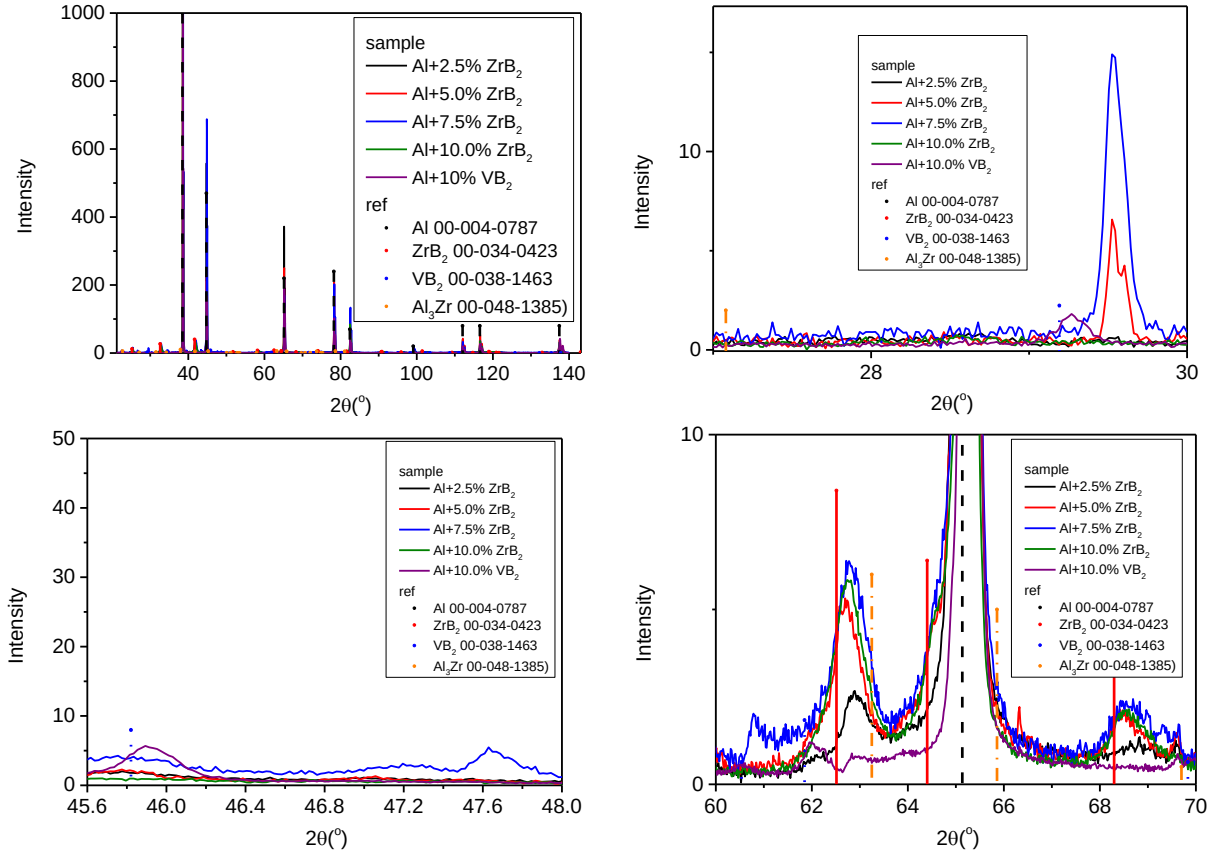

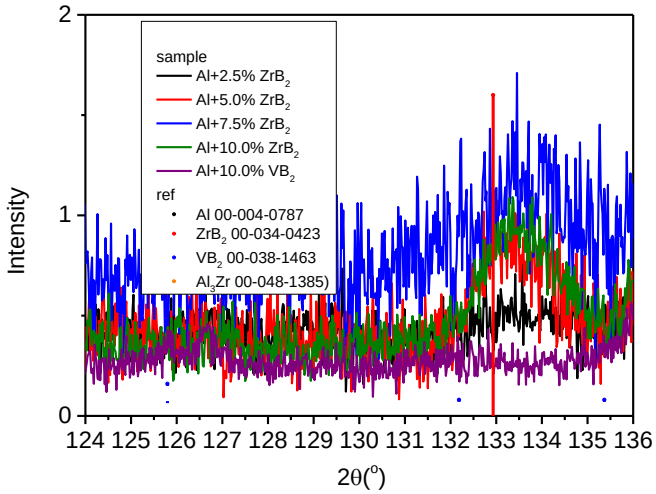

Figure 3.22 SEM analysis of AA6063/VB_2 composites with VB_2 peaks [36].

Using EDS Mapping (X-ray Energy Dispersive Mapping) on a composite with AA6063 reinforced with VB_2, the spatial distribution of the chemical elements present in the composite can be observed. This analysis technique allows mapping the chemical composition in different areas of the composite (Fig. 3.23).

The positions and distributions of VB_2 particles in the AA6063 aluminium matrix can be identified. This can provide information about how the VB_2 particles are distributed in the matrix and how they interact with the aluminium matrix.

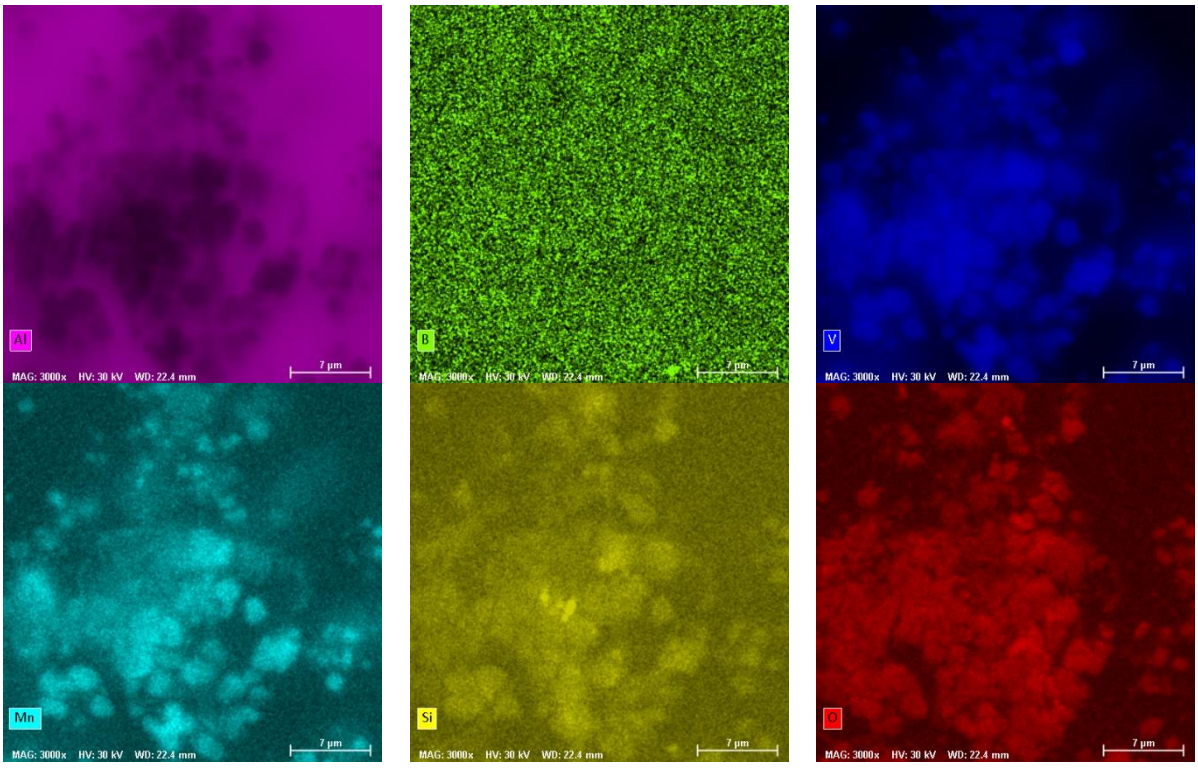

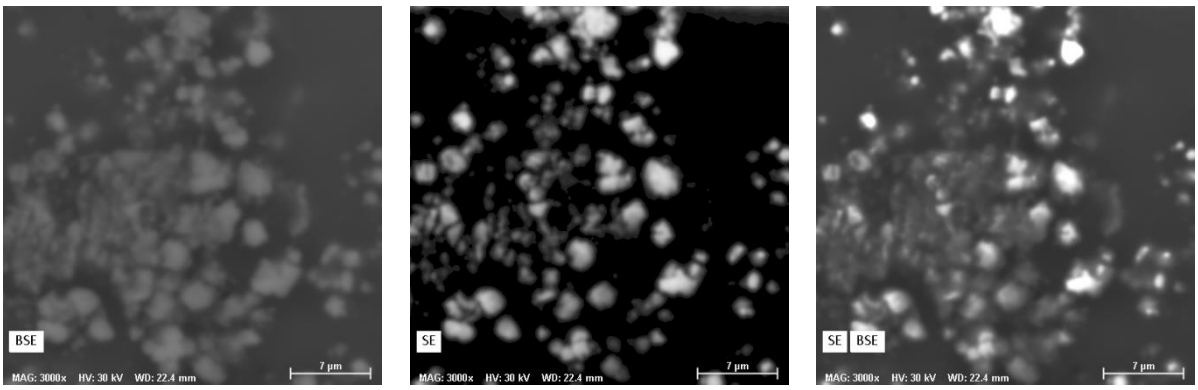

Map

Element	At. No.	Line s.	Netto	Mass [%]	Mass Norm. [%]	Atom [%]	abs. error [%] (1 sigma)	rel. error [%] (1 sigma)
Aluminium	13	K-Serie	377374117	164.40	86.93	90.38	8.22	5.00
Magnesium	12	K-Serie	4731943	2.07	1.10	1.26	0.12	5.76
Silicon	14	K-Serie	68327	0.03	0.02	0.02	0.00	4.48
Iron	26	K-Serie	681168	0.31	0.16	0.08	0.01	2.52
Titanium	22	K-Serie	828254	0.29	0.15	0.09	0.01	2.74
Zinc	30	K-Serie	4340	0.00	0.00	0.00	0.00	2.95
Copper	29	K-Serie	14937	0.01	0.00	0.00	0.00	2.61
Vanadium	23	K-Serie	48686473	16.94	8.96	4.93	0.45	2.66
Boron	5	K-Serie	0	0.00	0.00	0.00	0.00	10.00
Chromium	24	K-Serie	202456	0.08	0.04	0.02	0.00	2.62
Zirconium	40	L-Serie	533538	0.49	0.26	0.08	0.02	3.93
Oxygen	8	K-Serie	558180	3.18	1.68	2.95	0.33	10.54
Palladium	46	L-Serie	2683583	1.33	0.70	0.18	0.04	3.24
			Sum	**189.13**	**100.00**	**100.00**		

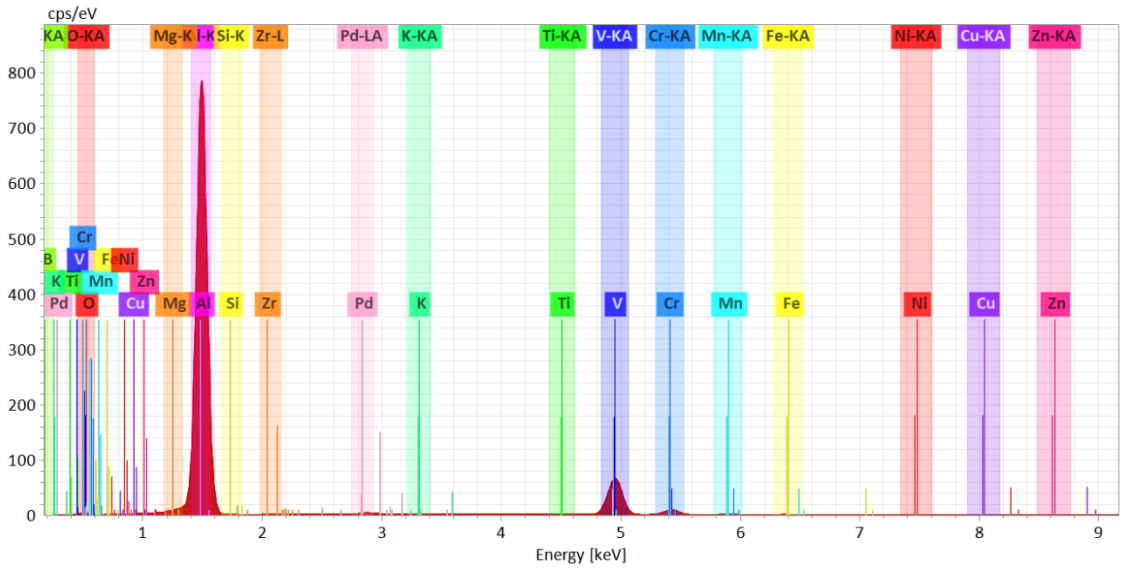

Figure 3.23 EDS MAPPING analysis [35]

Figure 3.24 illustrates the scanning electron microscope (SEM) analysis of the composite with a high concentration of VB_2, as well as the compositional analysis (EDS) of the vanadium (V)-containing particles. When the concentration of VB_2 particles was increased to 10%, their tendency to form agglomerations in certain areas was observed [35].

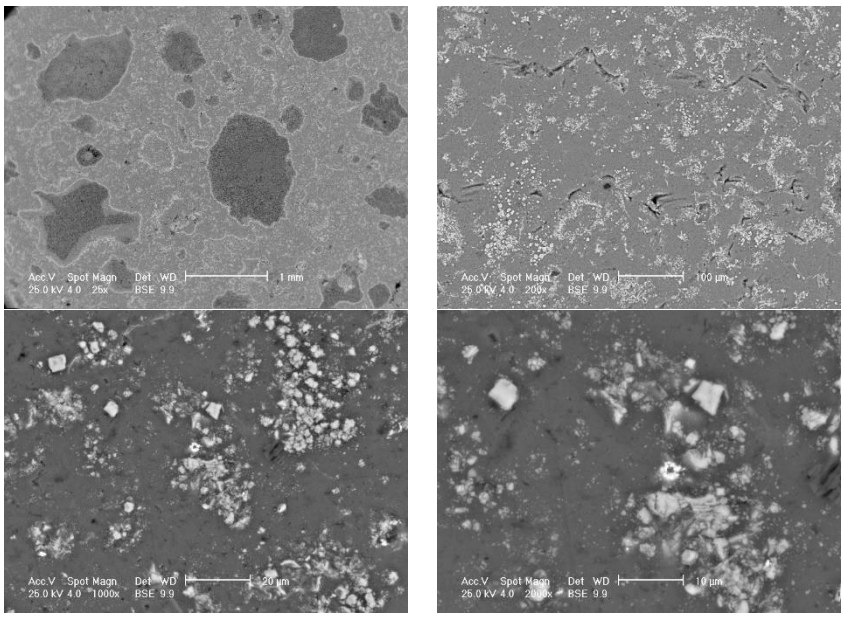

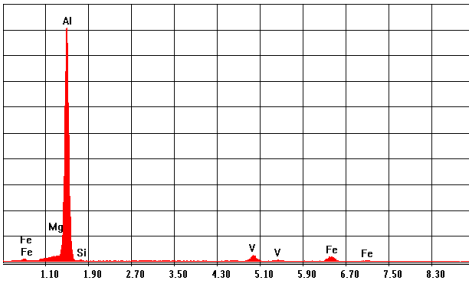

Element	Wt %	At %
MgK	2.33	2.73
AlK	86.7	91.36
SiK	0.22	0.22
V K	4.58	2.56
FeK	6.17	3.14
Total	100	100

EDS analysis (Polyhedral Particles) VB_2

Figure 3.24 Electron microscopy and EDS analysis of VB_2 particles [35]

During the analysis, we consulted the data resources available in the D8 ADVANCE diffractometer, specifically sheet 00-038-1463 for VB_2. This sheet provides detailed information on the crystallographic characteristics of VB_2, including the crystallographic systems in which it crystallizes, elemental cell parameters, interatomic distances, densities, molar masses, and more, relating to pure substances (Fig. 3.25).

00-038-1463 Dec 10, 2018 10:34 AM (ICDD)

Status Primary **Quality Mark:** Star **Environment:** Ambient **Temp:** 298.2 K **Chemical Formula:** V B2
Empirical Formula: B2 V **Weight %:** B29.80 V70.20 **Atomic %:** B66.67 V33.33
Compound Name: Boron Vanadium **CAS Number:** 12007-37-3 **Entry Date:** 09/01/1988

Radiation: CuKα1 (1.5406 Å) **Filter:** Graph Mono **Internal Standard:** Si **d-Spacing:** Diffractometer
Cutoff: 17.70 Å **Intensity:** Diffractometer - Peak

Crystal System: Hexagonal **SPGR:** P6/mmm (191)
Author's Cell [a: 2.99761(9) Å **c:** 3.05620(12) Å **Volume:** 23.78 Å³ **Z:** 1.00 **MolVol:** 23.78 **c/a:** 1.020]
Calculated Density: 5.066 g/cm³ **Color:** Dark gray **SS/FOM:** F(20) = 137.9(0.0073, 20)

Space Group: P6/mmm (191) **Molecular Weight:** 72.56 g/mol
Crystal Data [XtlCell a: 2.998 Å **XtlCell b:** 2.998 Å **XtlCell c:** 3.056 Å **XtlCell α:** 90.00° **XtlCell β:** 90.00°
XtlCell γ: 120.00° **XtlCell Vol:** 23.78 Å³ **XtlCell Z:** 1.00 **c/a:** 1.019 **a/b:** 1.000 **c/b:** 1.019]
Reduced Cell [RedCell a: 2.998 Å **RedCell b:** 2.998 Å **RedCell c:** 3.056 Å **RedCell α:** 90.00°
RedCell β: 90.00° **RedCell γ:** 120.00° **RedCell Vol:** 23.78 Å³]

Atomic parameters are cross-referenced from PDF entry 04-007-4807

Space Group Symmetry Operators:

Seq	Operator	Seq	Operator	Seq	Operator	Seq	Operator	Seq	Operator	Seq	Operator
1	x,y,z	5	-x+y,-x,z	9	-x,-x+y,z	13	-x,-y,z	17	x-y,x,z	21	x,x-y,z
2	-x,-y,-z	6	x-y,x,-z	10	x,x-y,-z	14	x,y,-z	18	-x+y,-x,-z	22	-x,-x+y,-z
3	-y,x-y,z	7	y,x,z	11	x-y,-y,z	15	y,-x+y,z	19	-y,-x,z	23	-x+y,y,z
4	y,-x+y,-z	8	-y,-x,-z	12	-x+y,y,-z	16	-y,x-y,-z	20	y,x,-z	24	x-y,-y,-z

Atomic Coordinates:

Atom	Num	Wyckoff	Symmetry	x	y	z	SOF	IDP	AET
V	1	1a	6/mmm	0.0	0.0	0.0	1.0		20-a
B	2	2d	-6m2	0.33333	0.66666	0.5	1.0		3#b

Crystal (Symmetry Allowed): Centrosymmetric

Subfiles: Common Phase, Inorganic, Metal & Alloy, NBS Pattern **Pearson Symbol:** hP3.00
Prototype Structure [Formula Order]: Al B2 **Prototype Structure [Alpha Order]:** Al B2
LPF Prototype Structure [Formula Order]: Al B2,hP3,191 **LPF Prototype Structure [Alpha Order]:** Al B2,hP3,191
ANX: NO2

Cross-Ref PDF #'s: 00-008-0118 (Deleted), ✓ 04-001-2358 (Primary), ✓ 04-001-2991 (Alternate), ✓ 04-002-0030 (Alternate), ✓ 04-002-0797 (Alternate), ✓ 04-002-8872 (Alternate), ✓ 04-003-2543 (Alternate), ✓ 04-003-6282 (Alternate), ✓ 04-004-5886 (Alternate), ✓ 04-006-2024 (Alternate), ✓ 04-007-4807 (Alternate)

References:

Type	DOI	Reference
Primary Reference		Wong-Ng, W., McMurdie, H., Paretzkin, B., Hubbard, C., Dragoo, A., NBS (USA). ICDD Grant-in-Aid (1986).
Crystal Structure		Crystal Structure Source: LPF.
Structure		1. Rudy, E., Benesovsky, F., Todt, L. Z. Metallkd. 54, 345 (1963).
Unit Cell		Wong-Ng, W., McMurdie, H., Paretzkin, B., Hubbard, C., Dragoo, A. Powder Diffr. 2, 115 (1987).

Database Comments: Additional Patterns: To replace 00-008-0118 (Paretzkin, Private Communication). ANX: NO2. Sample Source or Locality: The sample was obtained from Alfa Products, Thiokol/Ventron Division, Danvers, Massachusetts, USA, with a nominal purity of 99%. Structures: The structure was determined by Rudy et al. (1). Temperature of Data Collection: The mean temperature of data collection was 298.2 K. Unit Cell Data Source: Powder Diffraction.

d-Spacings (20) - V B2 - 00-038-1463 (Stick, Fixed Slit Intensity) - Cu Kα1 1.54056 Å

2θ (°)	d (Å)	I	h	k	l	*	2θ (°)	d (Å)	I	h	k	l	*
29.19127	**3.056720**	28	0	0	1		98.25279	1.018680	1	0	0	3	
34.53009	**2.595350**	71	1	0	0		102.28443	0.989180	3	2	0	2	
45.82088	**1.978670**	100	1	0	1		103.45740	0.981140	3	2	1	0	
60.53451	1.528230	8	0	0	2		108.64712	0.948243	4	1	0	3	
61.84841	1.498880	23	1	1	0		111.07780	0.934227	8	2	1	1	
69.83386	1.345730	8	1	1	1		125.79644	0.865290	2	3	0	0	
71.60209	1.316780	11	1	0	2		132.18374	0.842576	1	1	1	3	
72.81091	1.297870	6	2	0	0		135.36893	0.832639	1	3	0	1	
80.29028	1.194740	11	2	0	1		137.78956	0.825665	3	2	1	2	
92.07823	1.070110	9	1	1	2		147.96902	0.801384	2	2	0	3	

Figure 3.25. Sheet 00-038-1463 for VB_2

Isolation of VB_2 particles from composites was achieved by solubilization in a 35% hydrochloric acid (HCl) solution, followed by the appropriate filtration and dehydration procedures [36].

SEM analysis of the powders was performed using the SEM facility (VEGA II LMU) (Fig. 3.26). The SEM is a fully PC-controlled system equipped with a conventional tungsten-heated cathode with a maximum resolution of 5 nm @ 30 kV [36].

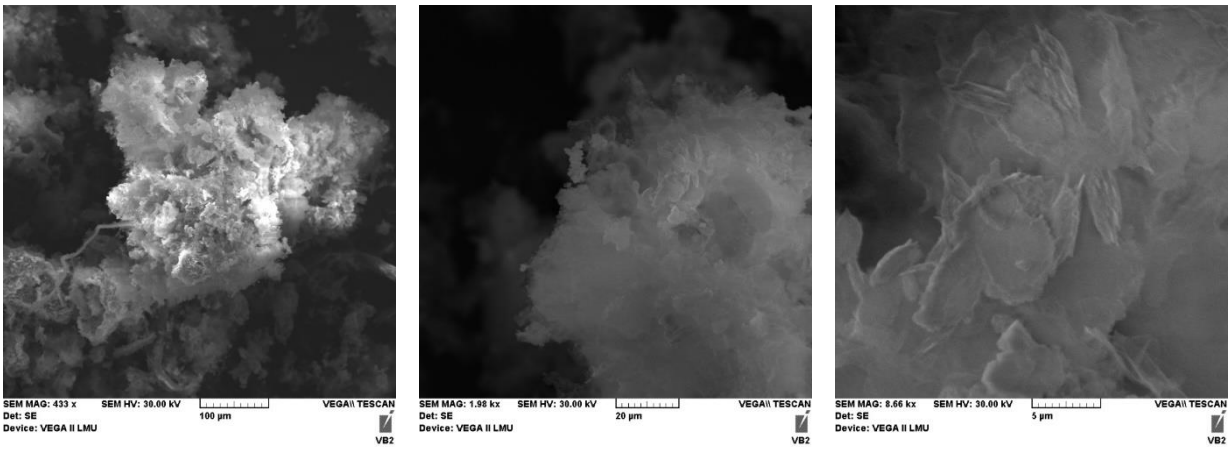

Figure 3.26 SEM images of VB_2 powders extracted from processed composite materials [36]

CHAPTER 4. Physico-mechanical properties of AA6063/VB_2 composites

The mechanical properties followed and determined for the developed composites were: hardness, mechanical strength at break, tensile strength, compressive strength.

Important properties of the reinforcement elements obtained in situ are shown in Table 4.1 [36].

Table 4.1. Physical properties of vanadium diboride [36]

IUPAC name	Theoretical chemical formula, [CASRN]	Crystal system, lattice parameters. Pearson symbol,	Thermal conductivity ($k.Wm^{-1}K^{-1}$)	Specific heat capacity ($c_p.J\ kg^{-1}\ K^{-1}$)	Coefficient of linear thermal expansion (α, $10^{-6}\ K^{-1}$)
Vanadium diboride	VB_2 [12007-37-3] 72.564	Hexagonal a = 0,2998 nm c = 0,3057 nm *hP*3, *P6/mmm*, AlB_2 type (Z = 1)	42,3	647,43	7,6-8,3

4.1. Hardness

Hardness was determined using a Leco M-400-G microhardness tester, year of manufacture 2004 used for Vickers hardness measurement and two INNOVATEST Model hardness testers: FALCON 500, year of manufacture 2015 and BUEHLER - WILSON, Model: REICHERTER UH 250, year of manufacture 2015.

$$HV_{med} = 2491,375$$

The operating principle of the Leco microhardness tester is to apply a load (P) for a specified duration of time (e.g. 100gf / 30 sec) to a diamond pyramid to produce a cavity of size (d). The resulting cavity size is measured using a calibrated optical microscope and the hardness is evaluated as the average applied stress (Fig. 4.1).

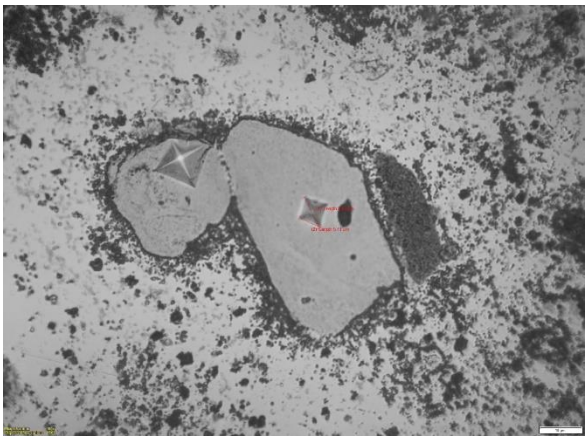

Figure 4.1 Determination of the size of cavities left after Vickers microhardness tests using optical microscopy measurement

• ***VB_2.*** Wear-resistant semiconductor films with density 5,070 g/cm3, melting temperature between 2450 ÷ 2747oC and Vickers hardness with values between 1750 and 4234 HV determined on particles obtained in-situ in composite AA6063/VB_2, with Leco M-400-G microhardness tester, averaging HV_{med} = 2491.

4.2. Tensile strength

Samples were taken from the specimens obtained for compositional characterisation and characterisation of the physical-mechanical properties.

Data for tensile strength and elongation were taken from the results obtained with the Instron Universal Testing Machine 8872 at room temperature using cylindrical specimens of 15 mm length and 5 mm diameter. On average, three specimens were used for each test.

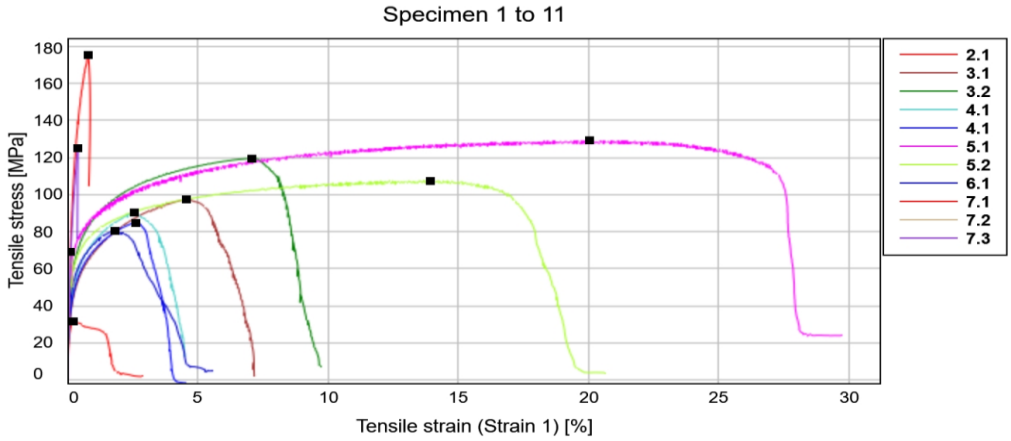

	Maximum Tensile stress [MPa]	Tensile strain (Strain 1) at Maximum Tensile stress [%]	Modulus (Segment 0.01 % - 0.02 %) [MPa]
1	31.39	0.25	44568.11
2	97.32	4.59	60130.13
3	119.46	7.11	70318.33
4	90.28	2.57	66660.06
5	84.87	2.62	65418.37
6	128.99	20.04	71281.04
7	107.51	13.92	67180.61
8	80.58	1.80	66622.26
9	175.56	0.81	79176.06
10	68.81	0.12	79484.16
11	124.69	0.40	76683.45

Figure 4.7 Tensile strength for all composite samples AA6063/VB_2

4.3. Compressive strength

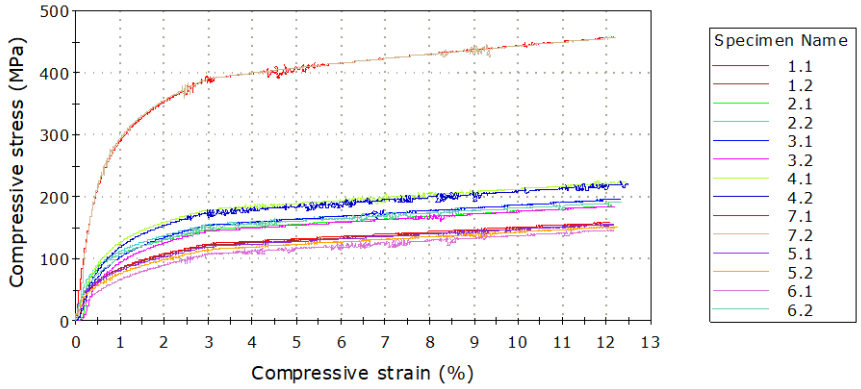

	Specimen label	Diameter (mm)	Anvil height (mm)	Modulus (Segment 0.1 % - 0.15 %) (MPa)
1	1.1	9.80000	15.10000	30617.17499
2	1.2	9.81000	14.00000	18194.80939
3	2.1	10.02000	15.11000	8700.41001
4	2.2	10.00000	15.05000	48821.12209
5	3.1	9.85000	15.03000	14251.73272
6	3.2	9.82000	15.20000	3472.24019
7	4.1	9.93000	15.20000	28332.52053
8	4.2	9.83000	15.10000	22483.93191
9	7.1	10.01000	14.90000	53292.16628
10	7.2	10.14000	15.17000	85591.78304
11	5.1	10.00000	14.98000	16851.39659
12	5.2	9.99000	15.08000	14304.94640
13	6.1	9.80000	15.20000	9009.85610
14	6.2	9.84000	15.20000	21494.25000

	Modulus (Segment 0.05 % - 0.15 %) (MPa)	Modulus (Segment 0.17 % - 0.27 %) (MPa)
1	28976.17925	13469.24064
2	19942.22697	9606.30191
3	4648.00278	47345.81666
4	39769.84488	15616.19999
5	12433.57746	21642.79971
6	2424.22845	18380.52876
7	28451.17130	22012.60604
8	17419.98954	23934.82594
9	59093.19946	45348.64477
10	57608.13377	54728.30928
11	21118.77748	8462.30480
12	17702.33701	7866.49249
13	9391.04219	7653.03388
14	22768.00432	12321.55325

Figure 4.14 Compressive strength for all composite samples AA6063/VB_2

4.4. DSC-TGA analysis

DSC-TGA analysis of composites with different concentrations of reinforcing elements The straight portion between 0 and about 100MPa can be seen on all curves σ = f(ε%) in compression, after which the samples move into the plastic range. Rupture occurs at high values of composite strain, increasing with increasing VB_2 content.

DSC analysis yields information on the peritectic transformation temperature at 660.452°C from the Al-V binary diagram.

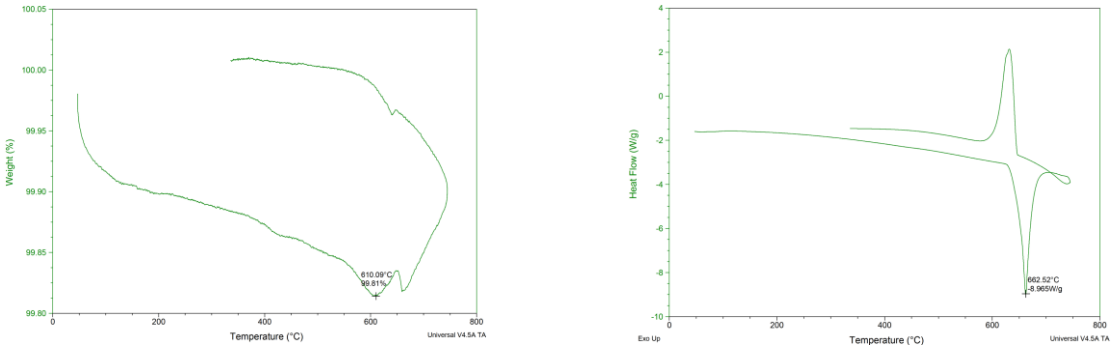

Figure 4.15 DSC (left) and TGA (right) analysis of AA6063 / 1% VB_2 composite

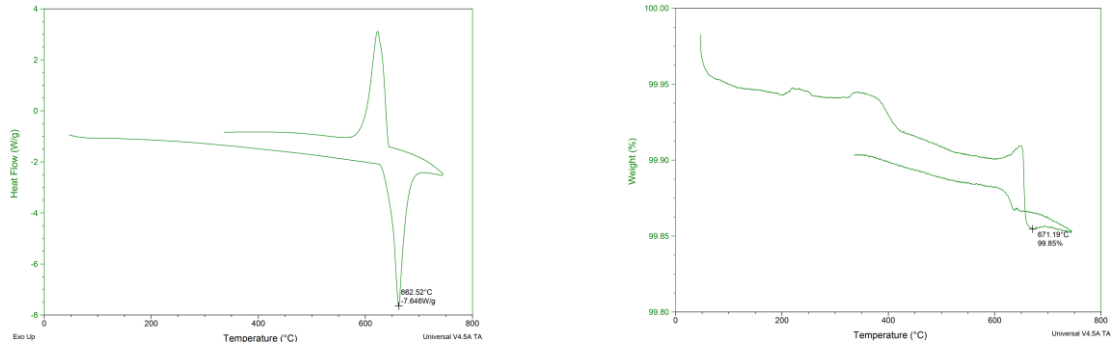

Figure 4.16 DSC (left) and TGA (right) analysis of AA6063 / 2% VB_2 composite

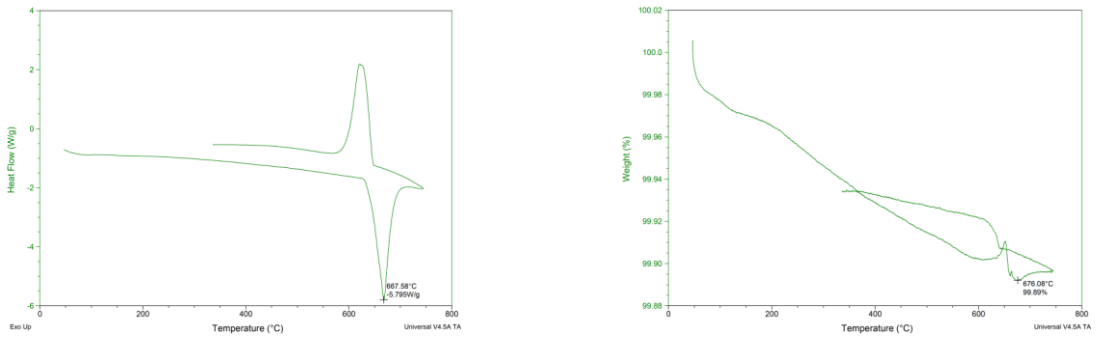

Figure 4.17 DSC (left) and TGA (right) analysis of AA6063 / 3% VB_2 composite

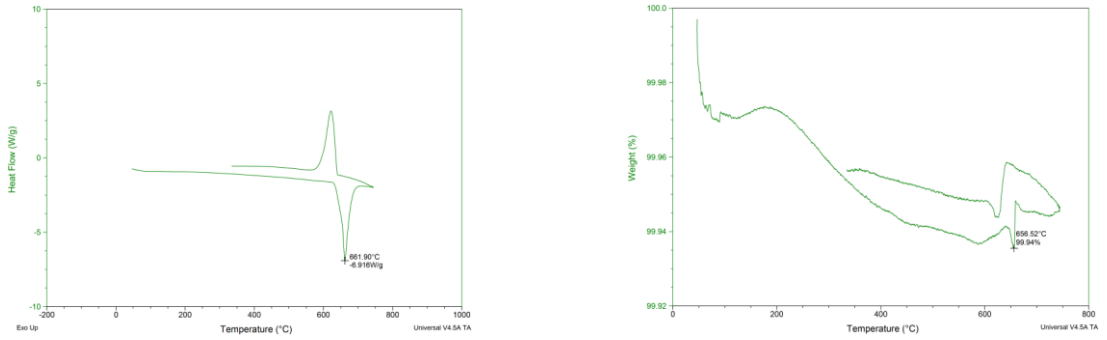

Figure 4.18 DSC (left) and TGA (right) analysis of AA6063 / 4% VB_2 composite

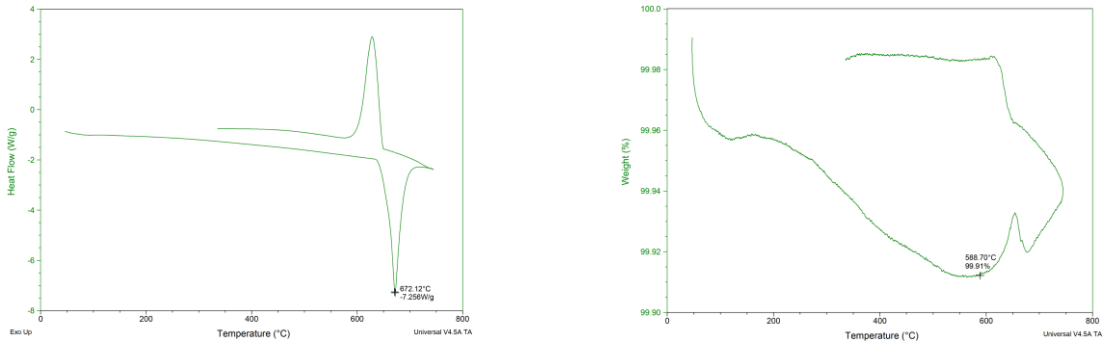

Figure 4.19 DSC (left) and TGA (right) analysis of AA6063 / 5% VB_2 composite

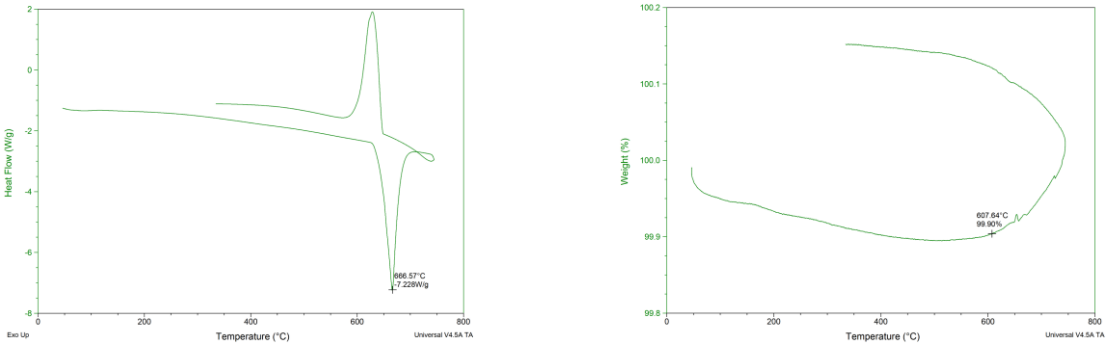

Figure 4.20 DSC (left) and TGA (right) analysis of AA6063/10% VB_2 composite

4.5. Tribological abrasion test

The resulting samples were subjected to an abrasive wear test using the CSEM CALOWEAR facility. The residual trace diameters from the abrasive wear test were determined by optical microscopy using the same Olympus UC30 equipment.

The measuring principle of the equipment is based on a rotating bearing steel ball with a diameter of d = 25 mm, which applies a certain load (F_N) on the tested surface.

DEVICE NAME	CSEM CALOWEAR
ABRASIVE PASTE	SiC
TEST PARAMETERS	• BALL DIAMETER: d=24.5 [mm] • BALL MATERIAL: special ball bearing steel • BALL PRESSING FORCE: F_N[N] • NUMBER OF REVOLUTIONS OF THE DRIVE SHAFT: n • TIME: t[s]

$$k = \frac{V}{F_N L_f} \; ; \quad V = \frac{\pi b^4}{32d}$$

where:

k = wear coefficient, $\left[\frac{mm^3}{Nm}\right]$

V = volume of wear, [mm^3],

b = the diameter left by the ball, [µm]

d = ball diameter, [mm]

Table 4.3 Processed abrasive wear test data for 1% VB_2 composite

Nr.crt	F_N [N]	F_N Ball [N]	n [rot]	t [s]	Vertical diameter [µm]	Horizontal diameter [µm]	Approximate surface area [μm^2]
1	0.355	0.538	4837	900	1460.58	1416.74	1684732
2	0.358	0.593	4837	900	1227.65	1363.30	1505392.55

Table 4.4 Processed abrasive wear test data for 2% VB_2 composite

Nr.crt	F_N [N]	$F_{N\ Ball}$ [N]	n [rot]	t [s]	Vertical diameter [µm]	Horizontal diameter [µm]	Approximate surface area [μm^2]
1	0.415	0.600	4837	900	1963.43	2082.63	3228928.31
2	0.410	0.607	4837	900	1374.26	1318.08	1372479.1

Table 4.5 Processed abrasive wear test data for 3% VB_2 composite

Nr.crt	F_N [N]	$F_{N\ Bila}$ [N]	n [rot]	t [s]	Vertical diameter [µm]	Horizontal diameter [µm]	Approximate surface area [μm^2]
1	0.377	0.490	4837	900	1403.30	1519.50	1478802.65
2	0.378	0.526	4837	900	1320.82	1204.36	1234357.31

Table 4.6 Processed abrasive wear test data for 4% VB_2 composite

Nr.crt	F_N [N]	$F_{N\ Bila}$ [N]	n [rot]	t [s]	Vertical diameter [µm]	Horizontal diameter [µm]	Approximate surface area [μm^2]
1	0.373	0.557	4837	900	1090.64	1089.27	962898.62
2	0.358	0.593	4837	900	1253.69	1156.41	1019322.70

Table 4.7 Processed abrasive wear test data for 5% VB_2 composite

Nr.crt	F_N [N]	$F_{N\ Bila}$ [N]	n [rot]	t [s]	Vertical diameter [µm]	Horizontal diameter [µm]	Approximate surface area [μm^2]
1	0.368	0.530	4837	900	1189.29	1192.03	1053431.85
2	0.366	0.545	4837	900	1303	1283.83	1133691.50

Table 4.8 Processed abrasive wear test data for 10% VB_2 composite

Nr.crt	F_N [N]	$F_{N\ Bila}$ [N]	n [rot]	t [s]	Vertical diameter [µm]	Horizontal diameter [µm]	Approximate surface area [μm^2]
1	0.408	0.595	4837	900	1509.91	1546.90	1900232.30
2	0.352	0.557	4837	900	1142.71	1131.74	1035079.35

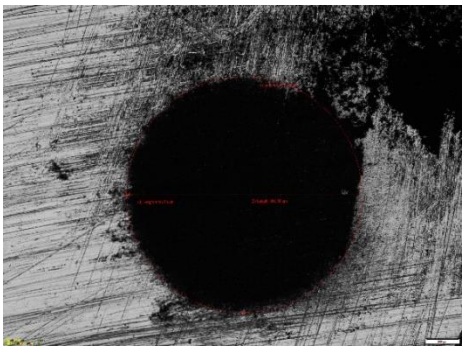

VB_2 1% x50

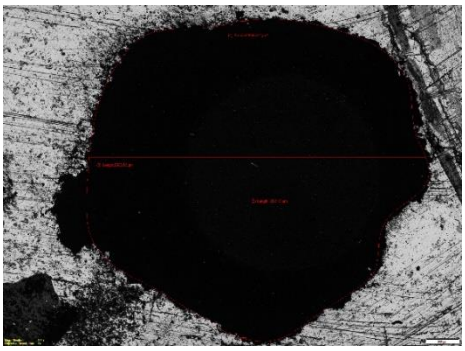

VB_2 2% x50

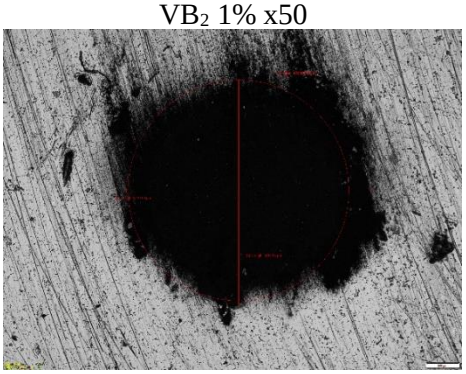

3% x50

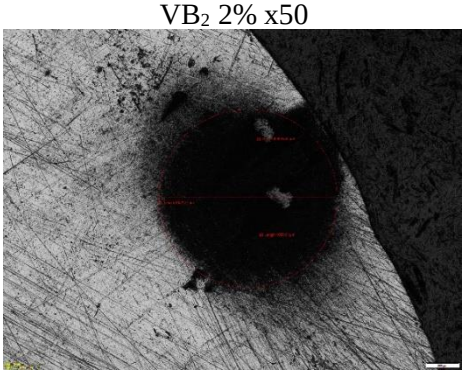

VB_2 4% x50

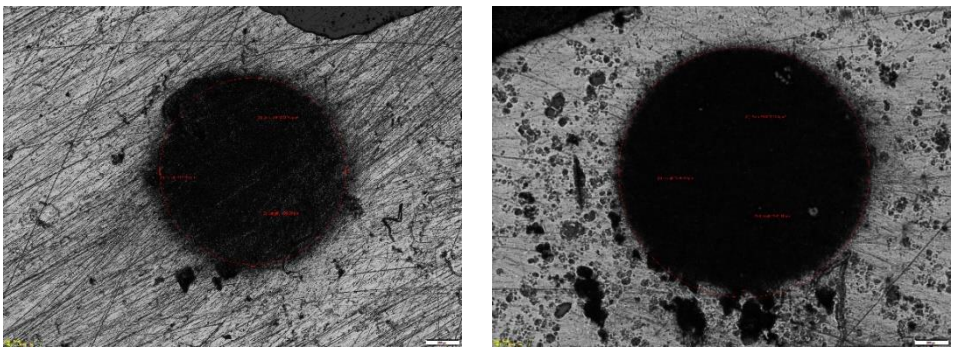

VB_2 5% x50 VB_2 10% x50

Figure 4.21 Optical microscopy analysis of abrasive wear test marks

Conclusions

The present work led to new materials with special properties obtained in-situ and the following results can be considered:

- Extensive literature study on composite materials - classifying them according to their basic matrix and reinforcing elements.
- Documentary study on the structure and properties of composite materials in comparison with the structure and properties of classical metallic materials.
- Thermodynamic study of the phenomena occurring in the AA6063 - AlV10 - KBF_4 - Na_3AlF_6 system during the aluminothermic reaction at different concentrations.
- Microstructural characterization of AA6063/VB_2 composite materials by optical and electron microscopy (SEM, TEM and HRTEM).
- Characterization of in-situ composites by X-ray diffraction (XRD) and energy dispersive spectroscopy (EDS) for different formed phases.
- TEM analysis of VB_2 compound to examine structure, composition and properties in detail.
- Vickers microhardness in different areas of composites reinforced with VB_2 ceramic particles.
- Tensile strength of composites reinforced with VB_2 ceramic particles.
- Compressive strength of composites reinforced with VB_2 ceramic particles.
- DSC-TGA analysis of composites with different concentrations of reinforcing elements.
- Tribological abrasion test of composites with different concentrations of reinforcing elements.

Bibliography

[1] COMPOSITE MATERIALS HANDBOOK, Volume 4 of 6 ed., Wichita State University: SAE International, 2013.

[2] P. K. Krishnan, J. V. Christy, R. Arunachalam, A.-H. I. Mourad, R. Muraliraja, M. Al-Maharbi, V. Murali și M. M. Chandra, „Production of aluminum alloy-based metal matrix composites using scrap aluminum alloy and waste materials: Influence on microstructure and mechanical properties," *Journal of Alloys and Compounds,* vol. 784, pp. 1047-1061, 2019.

[3] J. M. Mistry și P. P. Gohil, „Research review of diversified reinforcement on aluminum metal matrix composites: fabrication processes and mechanical characterization," *Science and Engineering of Composite Materials,* vol. 25, p. 633–647, 2018.

[4] S. K. Sharma, K. K. Saxena, V. Malik, K. A. Mohammed, C. Prakash, D. Buddhi și S. Dixit, „Significance of Alloying Elements on the Mechanical Characteristics of Mg-Based Materials for Biomedical Applications," *Crystals,* vol. 12, 2022.

[5] A. Gloria, R. Montanari, M. Richetta și A. Varone, „Alloys for Aeronautic Applications: State of the Art and Perspectives," *Metals,* vol. 9, nr. 662, pp. 1 - 26, 2019.

[6] COMPOSITE MATERIALS HANDBOOK, Wichita: SAE International, 2013.

[7] W. Hu, Z. Huang, Y. Wang, X. Li, H. Zhai, Y. Zhou și L. Chen, „Layered ternary MAX phases and their MX particulate derivative reinforced metal matrix composite:A review," *Journal of Alloys and Compounds,* vol. 856, p. 157313, 2021.

[8] N. Tamilselvam și S. Vijayakumar, „Reinforcements, Manufacturing Techniques, and Respective Property Changes of Al2O3/SiC Based Composites: A Review," *Silicon,* vol. 14, p. 3129–3146, 2022.

[9] G. Eckold, „Metal and Ceramic Matrix Composites," în *Design and Manufacture of Composite Structures,* Woodhead Publishing Series in Composites Science and Engineering, 1994, pp. 305-327.

[10] J. M. H. Ramirez, R. P. Bustamante, C. A. I. Merino și A. M. A. Morquecho, Unconventional Techniques for the Production of Light Alloys and Composites, Springer Cham, 2020.

[11] P. Moldovan, „Materiale de armare (ranforsare)," în *Compozite cu matrice metalică*, București, Printech, 2008, pp. 8-10.

[12] P. Moldovan, „Fibre scurte (discontinue) și whiskers-uri," în *Compozite cu matrice metalică*, București, PRINTECH, 2008, pp. 15-16.

[13] S. Seetharaman și M. Gupta, „Fundamentals of Metal Matrix Composites," în *Encyclopedia of Materials: Composites,* D. Brabazon, Ed., Oxford, Elsevier, 2021, pp. 11-29.

[14] M. C. Tanzi, S. Farè și G. Candiani, „Chapter 1 - Organization, Structure, and Properties of Materials," în *Foundations of Biomaterials Engineering*, M. C. Tanzi, S. Farè și G. Candiani, Ed., Academic Press, 2019, pp. 3-103.

[15] Z. Liu, G. Zu, H. Luo, Y. Liu și G. Yao, „Influence of Mg Addition on Graphite Particle Distribution in the Al Alloy Matrix Composites," *Journal of Materials Science & Technology,* vol. 26, pp. 244-250, 2010.

[16] M. Andre, U. A. Inam, R. T. Mousavian, D. Yan și B. Dermot, „Advanced production routes for metal matrix composites," *Engineering Reports,* vol. 3, nr. 5, 2020.

[17] „COMPOSITE MATERIALS HANDBOOK," în *VOLUME 4. METAL MATRIX COMPOSITES,* Wichita, SAE International, 2013.

[18] P. Moldovan, „Tehnici de producere in-situ," în *Compozite cu matrice metalică*, București, Printech, 2008, p. 124.

[19] P. Vishwakarma, R. Sekhar și T. Singh, „Finite element analysis of force variation with cutting speed in orthogonal turning of aluminum AA6351 alloy," *Int. J. Appl. Eng. Res.,* vol. 10, p. 10055–10064, 2015.

[20] V. Jatti, R. Sekhar și R. Patil, „Study of ball nose end milling of LM6 Al alloy: Surface roughness optimisation using genetic algorithm," *Int. J. Eng. Technol.,* vol. 5, p. 2859–2865, 2013.

[21] V. Jatti și R. Sekhar, „Surface Roughness Study on LM6 Al-Alloy: A Taguchi Approach," în *In Proceedings of the International Conference on Advanced Research in Engineering and Technology (ICARET 2013)*, Gunt, India, 2013.

[22] H. Xu și H. Huang, „Plasma remelting and injection method for fabricating metal matrix composite coatings reinforced with tungsten carbide," *Ceramics International,* vol. 48, nr. 2, pp. 2645-2659, 2021.

[23] Y. Li, K. Ramesh și E. Chin, „The compressive viscoplastic response of an A359/SiCp metal–matrix composite and of the A359 aluminum alloy matrix," *Int. J. Solids Struct.,* vol. 37, p. 7547–7562, 2000.

[24] Y. Li, K. Ramesh și E. Chin, „The mechanical response of an A359/SiCp MMC and the A359 aluminum matrix to dynamic shearing deformations," *Mater. Sci. Eng. A* , vol. 382, p. 162–170, 2004.

[25] P. Sivaprakasam, E. Abebe, R. Cep și M. Elangovan, „Thermo-Mechanical Behavior of Aluminum Matrix Nano-Composite Automobile Disc Brake Rotor Using Finite Element Method," *Materials,* vol. 15, nr. 6072, 2022.

[26] N. Ashrafi, A. H. Mohamed Ariff, D.-W. Jung, M. Sarraf, J. Foroughi, S. Sulaiman și T. S. Hong, „Magnetic, Electrical, and Physical Properties Evolution in Fe3O4 Nanofiller Reinforced Aluminium Matrix Composite Produced by Powder Metallurgy Method," *Materials,* vol. 15, 2022.

[27] P. Moldovan, „Microstructura MMC," în *Compozite cu matrice metalică*, București, Printech, 2008, pp. 68-69.

[28] T. Donomoto, N. Miura, K. Funatani și N. Miyake, „Ceramic fiber reinforced piston for high performance diesel engines," *SAE Paper No. 830252,* 1983.

[29] T. Yamauchi, „Development of SiC whiskers reinforced piston," *SAE Paper No. 911284,* 1991.

[30] T. Hayashi, H. Ushio și M. Ebisawa, „The properties of hybrid fiber reinforced metal and its application for engine block," *SAE Paper No. 890559,* 1989.

[31] Y. Nishida, Introduction to Metal Matrix Composites Fabrication and Recycling, Springer Tokyo: CORONA PUBLISHING CO., LTD. KINZOKUKI FUKUGOZAIRYO NYUMON, 2001.

[32] F. Murata, „Research and development of technology to promote recycling of aluminum materials," *J. Jpn. Inst. Light Met.,* vol. 46, p. 551–556, 1996.

[33] C. Carlos, O. Sergio și J. Pestana, „Effect of fiber length on the mechanical properties of high dosage carbon reinforced," *Procedia Structural Integrity,* vol. 5, pp. 539-546, 2017.

[34] F. Nturanabo, L. Masu și J. B. Kirabira, Novel Applications of Aluminium Metal Matrix Composites, London: IntechOpen, 2019.

[35] M. Butu, C. Ogica, D. F. Marcu, C. D. Stancel, F. Niculescu și V. D. Dragut, *OBTAINING OF AA6063/VB2 COMPOSITES PRODUCED BY ALUMINOTHERMIC REACTION,* vol. 83, 2021, p. 209–220.

[36] M. Butu, P. Moldovan, L. Rosu, C. Stancel, C. Ogica, L. Butu și M. Marinescu, „RESEARCH STUDIES ON OBTAINING METASTABLE INTERMETALLIC STRUCTURES IN 6xxx/BORIDES COMPOSITES," *UNIVERSITY POLITEHNICA OF BUCHAREST SCIENTIFIC BULLETIN SERIES B-CHEMISTRY AND MATERIALS SCIENCE,* vol. 82, p. 185–198, 2020.

[37] J. R. J. Quenisset și R. N. , „Wetting improvement of carbon or silicon carbide by aluminium alloys based on a K2ZrF6 surface treatment: application to composite material casting," *J. Mater. Sci.,* vol. 24, p. 2697–2703, 1989.

[38] M. Hansen, Constitution of binary alloy, New York: Metallurgy and Metallurgical Engineering Series, McGraw-Hill Book Company Inc., 1958.

[39] O. Barabaș și I. Kovali, Structura cristalină a metalelor și aliajelor, Kiev, 1989.

[40] O. Carlson, „The Al-B (Aluminum-Boron) System," *University Bulletin of Alloy Phase Diagrams,* vol. 11, nr. 6, 1990.

[41] H. Okamoto, „Al-B (Aluminum-Boron)," *Journal of Phase Equilibria and Diffusion,* vol. 27, nr. 2, 2006.

[42] M. Lee, B. Terry și P. Grieveson, „„ Interfacial phenomena in the reactions of Al-B, Al-Ti-B and Al-Zr-B alloys with KF-AlF3 and NaF-AlF3 melts,,” *Metallurgical Transactions B,* vol. 24B, 1993.

[43] Y. Birol, „Improved halide salt process to produce Al-B master alloys,” *Materials Science and Technology,* vol. 27, nr. 12, 2011.

[44] ASM Handbook, Binary Alloy Phase Diagrams, Volume 1, 1986.

[45] P. Villars, Pearson's Handbook of Crystallographic Data for Intermetallic Phases, 2nd Edition, ASM International, 1991.

[46] J. Daams, P. Villars și J. v. Vucht, Atlas of crystal structure for intermetallic phases, ASM International, 1991.

[47] J. Daams, P. Villars și J. v. Vucht, Atlas of crystal structure types, ASM International, 1991.

[48] D. Mirkovic, J. Gröbner, R. Schmid-Fetzer, O. Fabrichnaya și H. Lukas, „Experimental study and thermodynamic re-assessment of the Al-B system,” *Journal of Alloys and Compounds,* nr. 384, 2004.

[49] A. Khaliq, M. Rhamdhani, J. Mitchell, C. Davidson, G. Brooks și J. Grandfield, „ Analysis of Transition Metal (V, Zr) Borides Formation in Aluminium Melt,,” *https://www.researchgate.net/publication/258278390.*

[50] H. Duschanek și P. Rogl, „The Al-B (Aluminum-Boron) System, Phase Diagram Evaluations: Section II,” *Journal of Phase Equilibria,* vol. 15, nr. 5, 1994.

[51] J. Fjellstedt, A. Jarfors și L. Svendsen, „Experimental analysis of the intermediary phases AlB2, AlB12 and TiB2 in the Al-B and Al-Ti-B systems,” *Journal of Alloys and Compounds,* nr. 283, 1999.

[52] M. Lee, B. Terry și P. Grieveson, „Interfacial phenomena in the reactions of Al-B, Al-Ti-B and Al-Zr-B alloys with KF-AlF3 and NaF-AlF3 melts,” *Metallurgical Transactions B,* vol. 24B, 1993.

[53] ASM Handbook, Alloy Phase Diagrams, Volum 3, 1992.

[54] A. Kostov și D. Zivkovic, „Thermodynamic analysis of alloys Ti-Al, Ti-V, Al-V and Ti-Al-V,” *Journal of Alloys and Compounds,* nr. 460, 2008.

[55] W. Gong, Y. Du, B. Huang, R. Schmid-Fetzer, C. Zhang și H. Xu, „Thermodynamic reassessment of the Al-V System,” *Carl Hanser Verlag, München Z. Metallkd.,* nr. 95, 2004.

[56] B. Huber și K. Richter, „Observation of the new binary low temperatures compound Al-V,” *Journal of Alloys and Compounds,* nr. 493, 2010.

[57] J. Murray, „Al-V (Aluminum-Vanadium),” *Bulletin of Alloy Phase Diagrams,* vol. 10, nr. 4, 1989.

[58] H. Okamoto, „Al-V (Aluminum-Vanadium),” *Journal of Phase Equilibria and Diffusion,* vol. 33, nr. 6, 2012.

[59] M. Cevdet, „Physical and mechanical properties of cast under vacuum aluminum alloy 2024 containing lithium additions,” *Materials Research Bulletin,* vol. 35, pp. 1479-1494, 2000.

[60] Z. Hao, P. Rometsch, C. Lingfei și E. Yuri, „The influence of Mg/Si ratio and Cu content on the stretch formability of 6xxx aluminium alloys,” *Materials Science and Engineering: A,* vol. 651, 2015.

[61] M. Richard, A. Plotkowski, S. Amit, D. Ryan și B. Sudarsanam, „Towards high-temperature applications of aluminium alloys enabled by additive manufacturing,” *International Materials Reviews,* vol. 67, pp. 1-48, 2021.

[62] V. Zolotorevsky, N. Belov și M. Glazoff, Casting Aluminium Alloys, Elsevier Science, 2007.

[63] H. Philips, Annotated Equilibrium Phase Diagrams of Some Aluminum Alloy Systems, London: Inst. Met. Monograph 25, 1959.

[64] L. Mondol’fo, Aluminum Alloys – Structure and Properties, Boston: Butterworth, 1976.

[65] A. Slipenyuk, V. Kuprin, M. Yu, J. Spowart și D. Miracle, „The effect of matrix to reinforcement particle size ratio (PSR) on the microstructure and mechanical properties of a P/M processed AlCuMn/SiCp MMC.,” *Materials Science and Engineering: A.,* vol. 381, pp. 165-170, 2004.

[66] P. Oladijo, S. Awe, E. Akinlabi, R. Phiri, C. Lebudi și R. Phuti, „Encyclopedia of Materials: Composites," în *Reference Module in Materials Science and Materials Engineering*, Elsevier, 2021, pp. 360-374.

[67] I. Beckman, C. Lozano, E. Freeman și G. F. Riveros, „Selection for Reinforced Additive Manufacturing," *Polymers,* vol. 13, nr. 14, 2021.

[68] D. Wilson, „Fiber Strength," în *Encyclopedia of Materials: Science and Technology* , https://doi.org/10.1016/B0-08-043152-6/00557-X., Elsevier, 2001, pp. 3138-3142.

[69] N. Yoshinori, I. Norihisa și K. Yukio, „Recycling of aluminum matrix composites," *Metallurgical and Materials Transactions A,* vol. 30, pp. 839-844, 1999.

[70] D. Borjan, Ž. Knez și M. Knez, „Recycling of Carbon Fiber-Reinforced Composites-Difficulties and Future Perspectives," *Materials,* vol. 14, nr. 4191, 2021.

[71] T. Inoue, H. Inayoshi, H. Kanematsu, Y. Kunieda, S. Hayashi și T. Oki, „The recovery of aluminum from aluminum matrix composites by a molten salt process," *J. Jpn. Inst. Light Met.,* vol. 46, pp. 183-188, 1996.

[72] M. Malaki, A. Fadaei Tehrani, B. Niroumand și M. Gupta, „Wettability in Metal Matrix Composites," *Metals,* vol. 11, nr. 1034, 2021.

[73] A. Mortensen și J. Llorca, „Metal Matrix Composites," *Annual Review of Materials Research,* vol. 40, pp. 243-270, 2010.

[74] A. Rao și H. Cölfen, „Morphology control and molecular templates in biomineralization," în *Biomineralization and Biomaterials*, Woodhead Publishing, 2016, pp. 51-93.

[75] N. M. Nurazzi, M. Asyraf, S. Athiyah, S. Shazleen, S. Rafiqah, M. Harussani, S. Kamarudin, M. Razman, M. Rahmah, E. Zainudin, R. Ilyas, H. Aisyah, M. Norrrahim, N. Abdullah, S. Sapuan și A. Khalina, „A Review on Mechanical Performance of Hybrid Natural Fiber Polymer Composites for Structural Applications," *Polymers,* vol. 13, nr. 2170, 2021.

[76] K. Chawla, „Interfaces in metal matrix composites," *Composite Interfaces,* vol. 4, nr. 5, pp. 287-298, 1997.

[77] F. Kandil, J. Lord și A. Fry, A review of residual stress measurement methods-a guide to technical selection, Teddington, Middlesex, UK: NPL Materials Centre, 2001.

[78] J. Zhang și H. Zeng, „Intermolecular and Surface Interactions in Engineering Processes," *Engineering,* vol. 7, nr. 1, pp. 63-83, 2021.

[79] R. Everett, METAL MATRIX COMPOSITES: PROCESSING AND INTERFACES, Academic Press, 1991.

[80] W. Li, X. Yang, S. Wang, J. Xiao și Q. Hou, „Comprehensive Analysis on the Performance and," *Metals,* vol. 10, nr. 377, 2020.

[81] R. Sekhar, D. Sharma și P. Shah, „State of the Art in Metal Matrix Composites Research: A Bibliometric Analysis," *Appl. Syst. Innov.,* vol. 4, nr. 86, 2021.

[82] P. Xiao, Y. Gao, C. Yang, Y. Li, X. Huang, Q. Liu, S. Zhao, F. Xu și M. Gupta, „Strengthening and toughening mechanisms of Mg matrix composites reinforced with specific spatial arrangement of in-situ TiB2 nanoparticles," *Composites Part B: Engineering,* vol. 198, 2020.

[83] S. Tjong și Z. Ma, „Microstructural and mechanical characteristics of in situ metal matrix composites," *Mater Sci Eng R Rep,* vol. 3, pp. 49-113, 2000.

[84] P. Wang, C. Gammer, F. Brenne, T. Niendorf, J. Eckert și S. Scudino, „A heat treatable TiB2/Al-3.5Cu-1.5Mg-1Si composite fabricated by selective laser melting: microstructure, heat treatment and mechanical properties," *Compos B Eng,* vol. 147, pp. 162-168, 2018.

[85] W. Yu, S. Sing, C. Chua, C. Kuo și X. Tian, „Particle-reinforced metal matrix nanocomposites fabricated by selective laser melting: a state of the art review," *Prog Mater Sci,* vol. 104, pp. 330-379, 2019.

[86] M. El-Gallab și M. Sklad, „Machining of Al/SiC particulate metal-matrix composites: Part I: Tool performance," *Journal of Materials Processing Technology,* vol. 83, nr. 1-3, pp. 151-158, 1998.

[87] Z. Zhang, L. Zhang și Y. Mai, „Particle effects on friction and wear of aluminium matrix composites," *J Mater Sci,* vol. 30, p. 5999–6004, 1995.

[88] Y. Su, Q. Ouyang, W. Zhang, Z. Li, Q. Guo, G. Fan și D. Zhang, „Composite structure modeling and mechanical behavior of particle reinforced metal matrix composites," *Materials Science and Engineering: A,* vol. 597, pp. 359-369, 2014.

[89] J. Davis, „Aluminum and Aluminum Alloys," în *Alloying: Understanding the Basics,* ASM International, 2001.

[90] C. Zhang, Y.-P. Zeng, D. Yao, J. Yin, K. Zuo, Y. Xia și H. Liang, „The improved mechanical properties of Al matrix composites reinforced with oriented β-Si3N4 whisker," *Journal of Materials Science & Technology,* vol. 35, pp. 1345-1353, 2019.

[91] D. W. Richerson, „6.28 - Industrial Applications of Ceramic Matrix Composites," în *Comprehensive Composite Materials*, A. Kelly și C. Zweben, Ed., Oxford, Pergamon, 2000, pp. 549-570.

[92] Y. Liu, T. Zhao, W. Ju și S. Shi, „Materials discovery and design using machine learning," *Journal of Materiomics,* vol. 3, pp. 159-177, 2017.

[93] F. C. Campbell, „Chapter 1 - Introduction to Composite Materials and Processes: Unique Materials that Require Unique Processes," în *Manufacturing Processes for Advanced Composites*, F. C. Campbell, Ed., Amsterdam, Elsevier Science, 2004, pp. 1-37.

[94] A. Mussatto, I. U. I. Ahad, R. T. Mousavian, Y. Delaure și D. Brabazon, „Advanced production routes for metal matrix composites," *Engineering Reports,* vol. 3, p. e12330, 2021.

[95] J. E. Blendell și W. Rheinheimer, „Solid-State Sintering," în *Encyclopedia of Materials: Technical Ceramics and Glasses*, M. Pomeroy, Ed., Oxford, Elsevier, 2021, pp. 249-257.

[96] S. T. Mileiko, „Chapter XI - Hot Pressing," în *Metal and Ceramic Based Composites,* vol. 12, S. T. Mileiko, Ed., Elsevier, 1997, pp. 475-515.

[97] Y. G. Yushkov, E. M. Oks, A. V. Tyunkov și D. B. Zolotukhin, „Electron-Beam Synthesis of Dielectric Coatings Using Forevacuum Plasma Electron Sources (Review)," *Coatings,* vol. 12, 2022.

[98] P. Garg, A. Jamwal, D. Kumar, K. K. Sadasivuni, C. M. Hussain și P. Gupta, „Advance research progresses in aluminium matrix composites: manufacturing & applications," *Journal of Materials Research and Technology,* vol. 8, pp. 4924-4939, 2019.

[99] L. Liming, Z. Meili, P. Longxiu și W. Lin, „Studying of micro-bonding in diffusion welding joint for composite," *Materials Science and Engineering: A,* vol. 315, pp. 103-107, 2001.

[100] R. Chen, D. Zheng, T. Ma, H. Ding, Y. Su, J. Guo și H. Fu, „Effects and mechanism of ultrasonic irradiation on solidification microstructure and mechanical properties of binary TiAl alloys," *Ultrasonics Sonochemistry,* vol. 38, pp. 120-133, 2017.

[101] J. G. Speight, „Chapter 10 - Combustion of Hydrocarbons," în *Handbook of Industrial Hydrocarbon Processes*, J. G. Speight, Ed., Boston, Gulf Professional Publishing, 2011, pp. 355-393.

[102] S. C. Tjong și Z. Y. Ma, „Microstructural and mechanical characteristics of in situ metal matrix composites," *Materials Science and Engineering: R: Reports,* vol. 29, pp. 49-113, 2000.

[103] M. Malaki, A. Fadaei Tehrani, B. Niroumand și M. Gupta, „Wettability in Metal Matrix Composites," *Metals,* vol. 11, 2021.

[104] P. Moldovan, „Infiltrare reactivă," în *Compozite cu matrice metalică*, București, Printech, 2008, pp. 126-127.

[105] P. Moldovan, „Metode cu reactanți lichizi, solizi sau gazoși," în *Compozite cu matrice metalică,* București, Printech, 2008, pp. 125-126.

[106] M. Buțu și C. Stăncel, „Diagrame multicomponente," în *Compozite cu matrice metalică obținute prin reacții in situ,* București, Politehnica Press, 2021, pp. 68-69.